Review

Solid Electrolytes Based on NASICON-Structured Phosphates for Lithium Metal Batteries

Irina Stenina [iD]**, Svetlana Novikova** [iD]**, Daria Voropaeva** [iD] **and Andrey Yaroslavtsev** *[iD]

Kurnakov Institute of General and Inorganic Chemistry, Russian Academy of Sciences, Leninsky Prospekt, 31, Moscow 119991, Russia; stenina@igic.ras.ru (I.S.); svetlana_novi@mail.ru (S.N.); voropaeva-dd@yandex.ru (D.V.)
* Correspondence: yaroslav@igic.ras.ru; Tel.: +7-(495)-775-65-85

Abstract: All-solid-state lithium batteries are a promising alternative to commercially available lithium-ion batteries due to their ability to achieve high energy density, safety, and compactness. Electrolytes are key components of all-solid-state batteries, as they are crucial in determining the batteries' efficiency. Herein, the structure of $LiM_2(PO_4)_3$ (M = Ti, Ge, Zr) and lithium-ion migration mechanisms are introduced as well as different synthetic routes and doping (co-doping), and their influence on conductivity is discussed. The effective methods of reducing electrolyte/electrode interface resistance and improving ion-conducting properties are summarized. In addition, different polymer/NASICON composites are considered. The challenges and prospects of practical applications of NASICON-type lithium phosphates as electrolytes for all-solid-state batteries are discussed.

Keywords: solid electrolyte; NASICON; composite electrolyte; LAGP; LATP; lithium metal battery; all-solid-state battery; ionic conductivity

1. Introduction

The replacement of internal combustion engine vehicles with electric vehicles can provide significant reductions in greenhouse gas emissions and air pollution, and this is becoming a key strategy to minimize the carbon footprint of transportation. A growing number of car companies are now publishing their plans to achieve carbon neutrality in the coming decades, which means moving away from the production of internal combustion engine vehicles and moving towards electric vehicles. Such a transition requires scientific and technological advances in electrochemical power sources. Lithium-ion batteries are a key component of electric vehicles. To compete with internal combustion engines, batteries need to be safe, provide a range that is comparable to that of a car's internal combustion engine, and have a low cost. The automotive industry needs batteries with high energy density (450 Wh/kg and 900 Wh/L) and high power density for safe acceleration. Currently, lithium-ion batteries lead the way in electrochemical power sources, but to date, the achieved energy density for these devices is ~255 Wh/kg and close to the high point [1]. To increase energy density, it is necessary to improve the battery design and develop new uncommon electrochemical power sources, such as lithium metal batteries, lithium–air batteries, sodium-ion batteries, metal–sulfur batteries, etc.

All-solid-state lithium batteries (ASSLBs) with lithium metal anode and solid electrolyte are the most promising technology to achieve a high energy density of ~500 Wh/kg and reduce battery cost; hence, many automotive companies are actively investing in the development of lithium metal batteries. The high energy density of lithium metal batteries can be achieved due to the high theoretical specific capacity (~3860 mAh/g) and the low electrochemical potential of lithium (−3.04 V vs. standard hydrogen electrode) [1], and through the compactness of the battery design by using bipolar stacking in solid-state batteries, where the individual battery cells are connected in series through a single current collector in contact with the two electrodes without external connections (Figure 1) [2,3].

Such batteries have an operating temperature range from $-20\,°C$ to $+80\,°C$ and provide high charge/discharge rates [4].
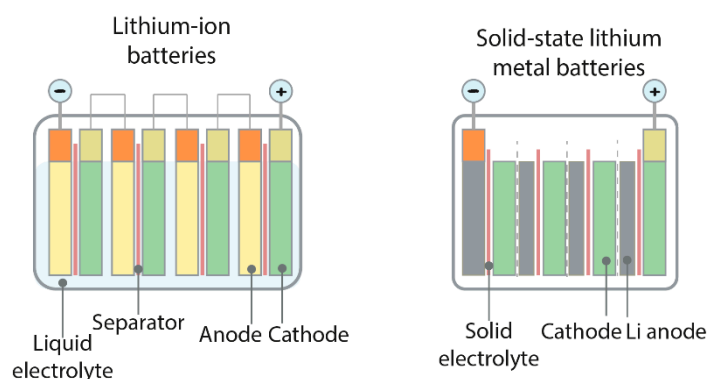

Figure 1. Schematic representation of a conventional lithium-ion battery and an ASSLB.

A crucial driver in the shift towards ASSLBs is the development of efficient solid-state electrolytes. An electrolyte provides ion transport and is one of the main components of an electrochemical device on which its capacity, power, operating temperature range, cyclability, and safety depend. The main requirements for solid electrolytes for batteries are a wide electrochemical stability window, high ionic conductivity and lithium transference numbers, and long-term cyclability. The main research in the field of solid electrolytes has focused on the following groups of materials: phosphates with the NASICON structure (NASICON is an acronym for Na super ionic conductor), garnets, perovskites, glass ceramics based on lithium phosphorus sulfide, and thin films based on LiPON [5–7]. Perovskites are generally very sensitive to moisture and CO_2 [8], and sulfide materials, despite having a high conductivity reaching 10^{-2} S/cm at room temperature [9], are highly hygroscopic and react with the moisture to form hydrogen sulfide, making them very difficult to handle under ordinary conditions [10]. Thus, phosphates with the NASICON structure and garnets seem to be the most promising electrolytes for ASSLBs.

Phosphates with the NASICON structure are air-stable and cheap. The general composition of these materials can be written as $[Li/Na]_{1+x}A_xB_{2-x}(XO_4)_3$, where A = Al, Cr, Fe, Nb, orTa; B = Ti, Ge, Sn, Zr, or Hf; and X = P or Si. Initially, sodium zirconium silicophosphates of compositions $Na_{1+x}Zr_2Si_xP_{3-x}O_{12}$, $0 < x < 3$ with ionic conductivity $> 10^{-1}$ S/cm at $300\,°C$ were called so [11,12]. Although the lithium conductivity of these materials is considerably inferior to that of sodium [13], the possibility of using them as solid electrolytes or cathode materials in lithium batteries has attracted the attention of many researchers [14–18]. Phosphates produced via heterovalent cation substitution are actively studied. This approach leads to the formation of vacancies in lithium positions or additional lithium ions in interstitials and provides a decrease in the transition temperature to highly conductive rhombohedral modification and an increase in ionic conductivity [19–21]. Thus, materials with the NASICON structure are among the most promising candidates for use as solid electrolytes in ASSLBs. However, the key issues limiting their application are chemical reactions with lithium metal, and poor contact at the electrode/electrolyte interface. Therefore, the purpose of this review is to summarize the recent results in improving the properties of phosphates with the NASICON structure and their application in ASSLBs.

2. Ionic Conductivity of Solid Electrolytes and Ways to Increase It

The total conductivity of solid electrolytes can be expressed as the sum of conductivities of different carriers [12] as follows:

$$\sigma = \sum N_i q_i u_i, \tag{1}$$

where N_i is the bulk concentration of carriers, q_i is the absolute value of their charge, and u_i is the mobility of carriers, which is equal to the average rate of their directional transport in an electric field.

In some ionic crystals, the ionic conductivity prevails, and the defects (vacancies and interstitials) act as electric carriers. This requires a high concentration of defects and their mobility. Mobility is determined by the nature of ions and their environment in the substance; thus, it is quite difficult to increase this value. Nevertheless, in the case of phosphates with the NASICON structure, increasing the mobility is possible by changing the composition that changes the size of the ion transport channels. Lang et al. used the density functional theory (DFT) to show that the substitution of Ti by iso- and aliovalent cations in $LiTi_2(PO_4)_3$ leads to changes in the size of LiO_6 octahedra, influencing lithium mobility [22]. Mutter et al. calculated the activation energies of Li migration using the vacancy mechanism for 18 compounds with the NASICON structure, namely $LiM_2(XO_4)_3$ (M = Zr, Ti, Hf, Fe, Nb, Ta, V, Ru, and Os, and X = P, Mn), using DFT [23]. It was shown that the activation energies are determined by the ionic neighborhood of the migrating ion. The authors deny that the factor limiting the mobility of the cations is the structural bottlenecks formed by triangularly arranged oxygen atoms. As of now, the main method of increasing the conductivity of solid electrolytes is increasing the concentration of charge carriers.

It should be noted that the conductivity of polycrystalline material σ_{tot} can be expressed as a parallel connection of the resistance $\rho_{surf||}$ characterizing the ionic transport along the interface surfaces with the successively connected bulk resistance of particles (ρ_{bulk}) and the resistance characterizing the ionic transport across the interface boundaries, perpendicular to the current direction ($\rho_{gb\perp}$) (Equation (2), Figure 2) as follows:

$$\sigma_{tot} = 1/(\rho_{bulk} + \rho_{gb\perp}) + 1/\rho_{suf||} \tag{2}$$
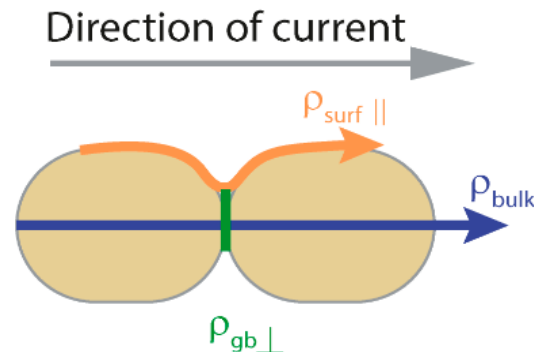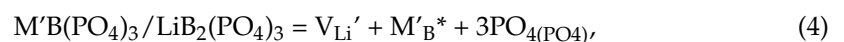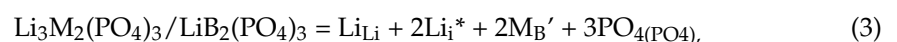

Figure 2. Ion transport in polycrystalline material.

Heterovalent doping, the use of nanoscale materials, and the formation of composites (see Section 4.3) are among the main approaches used to increase the ionic conductivity. These methods are based on the formation of point defects (vacancies and interstitials) in the crystal structure or at the interface, which act as electric carriers [24].

The formation of charged point defects in a crystal with the NASICON structure is exemplified by $LiB_2(PO_4)_3$ doped with trivalent (M, Equation (3)) and pentavalent cations (M′, Equation (4)). The defect formation can be described by the quasichemical reaction [25] as follows:

$$Li_3M_2(PO_4)_3/LiB_2(PO_4)_3 = Li_{Li} + 2Li_i{}^* + 2M_B{}' + 3PO_{4(PO4)}, \tag{3}$$

$$M'B(PO_4)_3/LiB_2(PO_4)_3 = V_{Li}{}' + M'_B{}^* + 3PO_{4(PO4)}, \tag{4}$$

where V is vacancies, and the superscripts * and ′ denote the positive and negative charges of the defects relative to the corresponding position in the lattice, respectively. The subscripts indicate the position of the ion in the lattice (B) or in the interstitials (i) [26]. When M^{3+} is introduced, its smaller positive charge (relative to the positions of the B^{4+} ions

in the lattice) is compensated by the incorporation of lithium ions into the interstitials (Equation (3)). The concentration of the latter must be equivalent to that of trivalent metal ions, replacing the tetravalent ones. When the pentavalent cation is introduced, its excess positive charge (relative to the positions of the B^{4+} ions in the lattice) is compensated by the formation of lithium vacancies (Equation (4)). This should lead to an increase in the defect concentration and bulk conductivity with an increase in the doping degree. On the other hand, the association of oppositely charged defects appears at a high doping degree due to electrostatic interaction, leading to a decrease in conductivity. Therefore, the dependence of conductivity on the doping degree most often passes through the maximum. It is well known that, due to their small size, lithium ions are preferentially moved by the interstitial mechanism. This is confirmed by both the results of ion transport modeling (DFT) and the experimental data for $LiTi_2(PO_4)_3$ phosphates with the NASICON structure [27]. The calculated activation energy for migrating lithium interstitials was found to be about 0.19 eV lower than that for migrating vacancies [22].

In the case of highly dispersed systems (nanomaterials), the defect formation on the particle surface occurs due to uncompensated chemical bonds [28–30]. The conditions of localization of the cations and anions on the particle surface differ significantly from those in the bulk. This results in the predominant sorption of cation vacancies or interstitials on the surface, and the oppositely charged defects are concentrated in a thin near-surface layer [31]. The surface charge arises on it and disappears in the bulk. The reactions of the formation of vacancies and interstitials on the surface (the subscript "S" denotes the position of the particle on the crystal surface) accompanied by the simultaneous presence or absence of metal ions in the bulk can be written as follows [24]:

$$M_M + V_S = M^*_S + V'_M \tag{5}$$

$$M^*_S + V_i = M^*_i + V_S \tag{6}$$

The lower binding of atoms to the surface and its high defectiveness leads to an increase in the translational mobility of ions and the acceleration of transport on the surfaces of the crystals for most inorganic ionic conductors [32,33].

According to numerous experimental data obtained via impedance spectroscopy, the bulk conductivity of phosphates with the NASICON structure significantly exceeds the grain boundary (in some cases, up to the order of magnitude) [34–38]. One possible reason for this phenomenon may be the violation of the contact between the particles due to low density. It seems reasonable to minimize the contribution of the grain boundary component to the total conductivity. Nakano et al. calculated grain boundary conductivities in $LiZr_2(PO_4)_3$ using molecular dynamics simulations with DFT-derived force field parameters for 32 grain boundary models consisting of various Miller indices and terminations [39]. Only some models showed improved Li-ion grain boundary conductivities compared to the bulk one [39]. Thus, the rational design of grain boundary structures can significantly improve Li-ion conductivity.

3. Structure and Ionic Conductivity of Materials Based on $LiB_2(PO_4)_3$ (B = Ti, Ge, Zr)

The NASICON structure for most of the compositions $[Li/Na]_{1+x}A_xB_{2-x}(XO_4)_3$ is characterized by rhombohedral syngony (space group R-3c), but its distortion to monoclinic or triclinic syngony is possible. The $[Li/Na]_{1+x}A_xB_{2-x}(XO_4)_3$ structure is composed of tetrahedra XO_4 (SiO_4 and PO_4) and BO_6 (AO_6) octahedra, which are connected to each other by common vertices in a three-dimensional framework (Figure 3). The latter has cavities available to host lithium or sodium ions. In the rhombohedral modification, single-charged M^+ cations (M = Li, Na) can occupy positions 6b and 18e, denoted as M1 and M2, respectively, forming a three-dimensional M1–M2–M1 conduction pathway. Monoclinic modification is thought to be formed by distorting the rhombohedral structure in which the M2 positions are split into two M2 and M3 positions. Accordingly, it becomes possible to

move lithium (sodium) along two pathways, M1–M2–M1 and M1–M3–M1. When lithium (sodium) ions occupy only one type of M1 site (for example, in $NaZr_2(PO_4)_3$), the activation energy of single-charged ion transport is high due to a low defect concentration.
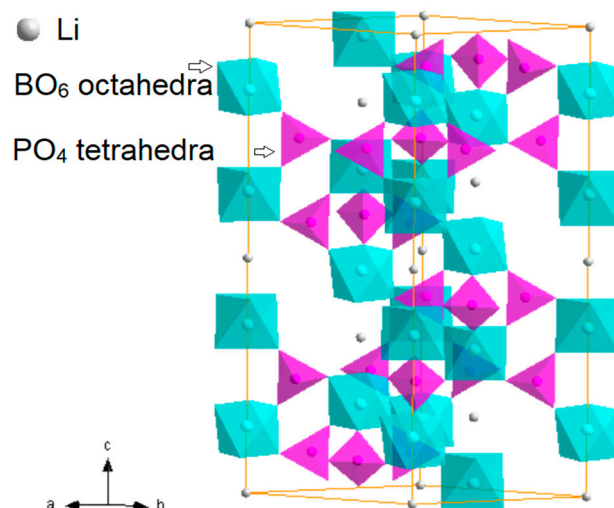

Figure 3. Scheme of NASICON-type crystal structure (R-3c).

In the case of heterovalent doping (for example, in the case of the replacement of a part of B^{4+} by trivalent cations), to compensate for the local violation of the electroneutrality of a lattice, additional single-charged cations should be introduced into a structure according to Equation (3). These ions partially occupy the M2 or M3 positions, as in $Li_{1+x}Al_xTi_{2-x}(PO_4)_3$ [40], and the activation energy of lithium (sodium) ion transport is reduced by reducing the electrostatic repulsion between them. In addition, ion diffusion in the NASICON structure is limited by the size of the tunnel's narrow spots ("bottle necks" in the transport path of the mobile ion), which is determined by the B ions that make up the three-dimensional framework. Thus, by selecting suitable frame-forming ions, including changing their content during doping, the ionic conductivity of the solid electrolyte can be significantly increased. Hereafter, the conductivity of some lithium-conducting materials based on $LiB_2(PO_4)_3$ (B = Ti, Ge, Zr) will be discussed in detail.

3.1. Materials Based on $LiTi_2(PO_4)_3$

Lithium titanium phosphate $LiTi_2(PO_4)_3$ attracts the greatest attention among phosphates with the NASICON structure despite the low value of lithium conductivity at room temperature (~10^{-7} S/cm). A partial replacement of titanium by tri- or pentavalent cations can significantly increase the ionic conductivity (up to 10^{-4}–10^{-3} S/cm) [25,41,42]. For example, it was reported that the conductivity of solid solution $Li_{1+x}Cr_xTi_{2-x}(PO_4)_3$ was close to 10^{-3} S/cm at room temperature [25].. A high concentration of charge carriers plays a key role in increasing conductivity. However, the possibility of optimizing the size of the channels for lithium-ion migration is also noted. Therefore, increasing the channel size in $LiTi_2(PO_4)_3$ via a partial replacement of titanium with zirconium ($LiTi_{2-x}Zr_x(PO_4)_3$) [43,44] or germanium ($LiTi_{2-x}Ge_x(PO_4)_3$) leads to a significant increase in its conductivity at room temperature [45].

Researchers pay the greatest attention to $Li_{1+x}Al_xTi_{2-x}(PO_4)_3$ (LATP), where Ti^{4+} ions are partially replaced by Al^{3+} [46,47]. Such materials are the subject of the following reviews [18,48–51]. On the basis of mathematical simulations, it was found that the ionic conductivity of LATP significantly depends on the aluminum content, which is caused by the structure of the material [49]. At a high Al content, the non-conducting $AlPO_4$ phase is formed at the grain boundaries and negatively affects the ionic conductivity [52,53]. The maximum ionic conductivity (7×10^{-4} S/cm at 25 °C) is achieved at the optimal aluminum content x = 0.3–0.4 [52,54].

The microstructure, porosity, and interfaces have a significant influence on the conductive properties of the materials described above. Therefore, the most important task is to reduce the contribution of the interfaces. It was shown that by introducing various types of additives such as Li_2O [55,56], B_2O_3 [56–58], etc., concentrated at the interfaces, the density of phosphate-based ceramics with the NASICON structure is significantly improved. The use of additives with intrinsic conductivity, such as $LiBO_2$ or Li_3PO_4, can improve the conductivity of the resulting electrolytes [56,59]. Thus, the conductivity of the $LiTi_2(PO_4)_3$-$0.2Li_3BO_3$ system at 25 °C reaches 3.0×10^{-4} S/cm, which is several orders of magnitude higher than the conductivity of lithium titanium phosphate [60].

3.2. Materials Based on $LiGe_2(PO_4)_3$

Much attention has also been paid to lithium germanium phosphate. A wide range of materials based on lithium germanium phosphate doped with trivalent cations (Al, Cr, Ga, Fe, Sc, and In) was studied in [61]. The maximum conductivity was observed for $Li_{1+x}Al_xGe_{2-x}(PO_4)_3$ (LAGP), where x = 0.4–0.7. Most studies report that the conductivity of these materials is equal to $(1.0–5.8) \times 10^{-4}$ S/cm at room temperature [62–65]. The value of the bulk conductivity of $Li_{1.5}Al_{0.5}Ge_{1.5}(PO_4)_3$ was shown to be 1×10^{-3} S/cm at room temperature [35]. The ionic conductivity of solid electrolytes based on phosphates with the NASICON structure depends on the nature of the doping ion and its content, the presence of impurity phases, and the synthesis method. The use of a liquid phase precursor based on water-soluble Ge(IV) oxalate showed the optimal synthesis temperature (up to 650 °C) and the preparation time of $Li_{1.5}Al_{0.5}Ge_{1.5}(PO_4)_3$ powders due to a better homogenization of the reaction mixture [35]. The single-phase powder of $Li_{1.5}Al_{0.5}Ge_{1.5}(PO_4)_3$ without the non-conducting impurities GeP_2O_7 and GeO_2 was formed after sintering the precursor at 650 °C. Another promising way to increase the ionic conductivity of LAGP may be to lower the porosity of the materials by obtaining glass ceramics—composites that simultaneously contain a glassy and a crystalline phase. If the latter is formed by nanoparticles, this leads to a high conductivity of the materials obtained. Such materials with a high grain boundary conductivity can have significant advantages [66]. In this context, there has been increased focus on systems that are similar in composition to NASICONs [67,68].

3.3. Materials Based on $LiZr_2(PO_4)_3$

The use of materials based on $LiZr_2(PO_4)_3$ (LZP) can be very promising. The ionic conductivity of this compound is 3×10^{-6} S/cm at room temperature. However, when heated above 40 °C, there is a marked increase in the conductivity, and at 300 °C, its value reaches 1.2×10^{-2} S/cm. The observed phenomenon is associated with a phase transition that occurs at 40–55 °C, accompanied by a change from a monoclinic structure to a rhombohedral structure [69]. Doping the material with trivalent cations (scandium, indium, etc.) can stabilize the highly conductive rhombohedral modification already at room temperature [70]. There are also results of the successful substitution of zirconium cations in $LiZr_2(PO_4)_3$ for divalent calcium and strontium cations, and trivalent yttrium cations [71–75]. At the same time, the conductivity of some of the obtained materials was close to that of $LiTi_{2-x}Al_x(PO_4)_3$ (0.3 < x < 0.4).

3.4. Effect of the Synthesis Method on the Ionic Conductivity of Phosphates with the NASICON Structure

The method of solid electrolyte preparation has a great influence on the characteristics of the resulting materials, including their ionic conductivity, particle size, activation energy, and ceramic density [76]. Phosphates with the NASICON structure can be obtained using solid-state techniques (classical solid-state synthesis, melt quenching with subsequent crystallization) or using the liquid phase, including co-precipitation and sol-gel methods.

Solid-phase synthesis is the traditional method for producing LAGP, LATP, and LZP [46]. Precursors (Al_2O_3, GeO_2, Li_2CO_3, and $(NH_4)_xH_yPO_4$ for LAGP; Al_2O_3, TiO_2, Li_2CO_3, and $(NH_4)_xH_yPO_4$ for LATP; and Li_2CO_3, $Zr(HPO_4)_2 \cdot H_2O$, and ZrO_2 for LZP [70])

are completely mixed and ground in a ball mill, followed by a solid-phase reaction and particle densification via calcination and sintering, which generally require high temperatures (700–1200 °C) and long holding times (>12 h). In solid-phase synthesis, starting reagents can be pressed into pellets and sintered directly during synthesis. The samples prepared using this method usually have a highly crystalline structure, large grains, and high ionic conductivity and density.

In the melt-quenching method, the precursors are first melted at a high temperature (>1200–1500 °C [77–79]) and rapidly cooled down to room temperature. The resulting amorphous glass is subsequently sintered as LAGP or LATP glass-ceramic. LAGP and LATP melted–hardened glass-ceramics were reported to exhibit the high Li-ion conductivity of 4.22×10^{-3} and 1×10^{-3} S/cm at room temperature, respectively [80,81]. The introduction of various additives during glass crystallization can further improve the microstructure of the resulting materials [77,82,83]. This approach, which makes it possible to produce glass-ceramic materials, seems especially promising for germanium-containing phosphates [84].

Wet chemistry methods, in comparison to solid-phase synthesis and melt quenching, require lower heat treatment temperatures and achieve better control of the particle size and morphology of LATP and LAGP solid electrolytes. The sol-gel method offers an efficient way to synthesize crystalline LATP and LAGP solid electrolytes, using an intermediate step with a solvent to form a colloidal solution, then a gel network, followed by heat treatment for crystallization. Using the sol-gel method, pure materials can be obtained at lower temperatures and shorter times compared to solid-phase synthesis and melt quenching [46].

The co-precipitation method often involves dissolving the desired precursors in an aqueous solution, followed by precipitation at a controlled pH [85]. After co-precipitation, the obtained powders are subjected to medium- and high-temperature sintering.

Synthesized phosphate powders with the NASICON structure are sintered to produce denser ceramics. An additional physical treatment, such as spark plasma sintering (SPS) [78,81,86,87] or microwave processing [79,88] are used to reduce the temperature and final sintering time. The use of such processes ensures a tighter adhesion of particles to solid surfaces [89]. The results of the synthesis of ceramics $Li_{1.3}Al_{0.3}Ti_{1.7}(PO_4)_3$ via SPS are reported in ref. [47]. The densification of materials via SPS (sintering temperature 900 °C; sintering time 5 min) allows for the formation of ceramics with a density of 97–98% with a high lithium-ion conductivity ($\sigma_{total} = 2.9 \times 10^{-4}$ S/cm and $\sigma_{bulk} = 1.6 \times 10^{-3}$ S/cm) [47].

Figure 4 shows the effect of the synthesis method on the ionic conductivity of electrolytes using LATP and LAGP materials as examples. It should be noted that it is difficult to quantitatively compare the ionic conductivities obtained in different works and to evaluate the effect of the synthesis method on transport properties due to the differences in the source materials, the purity of reagents, the heating rates, etc. Generally, the liquid-phase and melt-quenching methods allow for the achievement of a high ionic conductivity of a material. The use of the liquid-phase method often allows for the microstructure and morphology of powders to be adjusted, which provides a higher ionic conductivity. The melt-quenching technique produces materials with a high ionic conductivity but requires high temperatures.
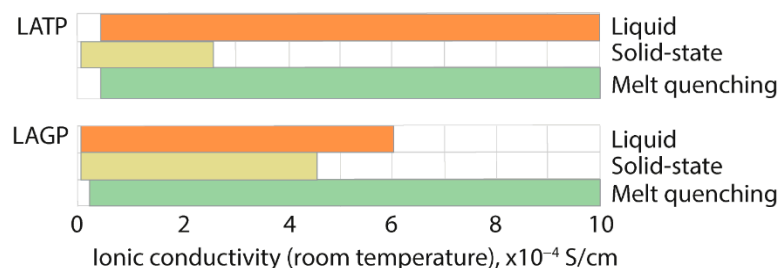

Figure 4. Ionic conductivity range of LAGP and LATP electrolytes depending on the synthesis method; liquid-phase [86,90–100], solid-state [87,88,101], and melt-quenching techniques [68,78,79,102–110].

3.5. Co-Doping of LATP and LAGP

Most research papers about the conductive properties of compounds with the NASICON structure report doping with one type of cation with a lower valence, which allows for the increase in the concentration of single-charged lithium ions in the interstitials (the most mobile charge carriers in this structure). At the same time, the highest conductivity of one of the most well-known solid electrolytes, zirconia, was achieved via simultaneous doping with two types of cations (co-doping) [111]. This approach can also be effective in increasing the ionic conductivity of phosphates with the NASICON structure. Obviously, the aim of heterovalent substitution is to increase the concentration of carriers. Generally, a positive effect of heterovalent doping is observed only for low degrees of substitution (doping degrees). With an increase in the doping degree, the defect association is observed; the formation of impurity phases that are sorbed at interfaces is possible, which leads to a decrease in conductivity. In the case of co-doping, these effects can be exacerbated. The aim of isovalent substitution is not so obvious and implies the optimization of the size of conductive channels, as in the substitution of a part of titanium for larger zirconium [43,112]. However, it is also possible to increase the conductivity by replacing a part of titanium with germanium that has a smaller ion size [45].

To date, there are relatively few data on the co-doping of lithium phosphates with the NASICON structure. Most of the works are devoted to phosphates based on $LiTi_2(PO_4)_3$ co-doped with aluminum and germanium [113–117]. The idea of a partial replacement of Ti^{4+} by Al^{3+} and Ge^{4+} ions was to combine the high conductivity of $Li_{1+x}Al_xTi_{2-x}(PO_4)_3$ with the better chemical stability of $Li_{1+x}Al_xGe_{2-x}(PO_4)_3$. Generally, co-doping does not affect the chemical stability of doped materials. However, the introduction of certain elements can lead to its increase; e.g., the change in the titanium content in the $Li_{1+x}Al_xTi_{2-x-y}Ge_y(PO_4)_3$ system can influence the electrolytic properties of materials due to a stronger covalency of the Ge–O bond than that of the Ti–O bond [116]. At the same time, if we are talking about the stability of co-doped NASICONs when in contact with a Li metal anode, there is no such effect (see also Section 4 below). For example, none of the samples $Li_{1+x-y}Al_x^{3+}M_y^{5+}M_{2-x-y}^{4+}$ $(PO_4)_3$ (M^{4+} = Ti, Ge, and M^{5+} = Ta) are stable when in contact with lithium [118]. Among the materials $Li_{1.4}Al_{0.4}Ti_{1.6-x}Ge_x(PO_4)_3$ (x = 0–1.0) obtained using the sol-gel method following sintering at 900 °C, the sample $Li_{1.4}Al_{0.4}Ti_{1.4}Ge_{0.2}(PO_4)_3$ showed the highest conductivity (1.3×10^{-3} S/cm at 25 °C) [113]. It exhibited stability in saturated LiOH and LiCl solutions and can be used as a protective layer for Li metal electrodes in aqueous lithium–air batteries [113]. The conductivity of $Li_{1+x}Al_xTi_{2-x-y}Ge_y(PO_4)_3$ ($0.2 \leq x \leq 0.8$, y = 0.8, 1.0) obtained using the solid-state method at 950 °C reaches $(2-7) \times 10^{-4}$ S/cm at room temperature [117]. Nuernberg et al. reported that increasing the lithium content in $Li_{1+x}Cr_xGeTi_{1-x}(PO_4)_3$ ($0 \leq x \leq 1$) with a partial replacement of Ti^{4+} by Cr^{3+} leads to the occupation of position 36f (Li3) followed by a partial release of position 6b (Li1) [119]. The co-doping of lithium titanium phosphate with aluminum and tin ions leads to an increase in conductivity by up to 4.7×10^{-4} S/cm at room temperature for $Li_{1.3}Al_{0.3}Sn_{0.35}Ti_{1.35}(PO_4)_3$ due to the achievement of the optimal ion transport channel size [120]. In the case of co-doping with aluminum and zirconium ions, the highest ionic conductivity was observed for $Li_{1.2}Al_{0.2}Zr_{0.1}Ti_{1.7}(PO_4)_3$ (7.9×10^{-4} S/cm) [121] and $Li_{1.3}Al_{0.3}Ti_{1.6}Zr_{0.1}(PO_4)_3$ (2.3×10^{-5} S/cm) [122]. To date, the highest ionic conductivity (6.6×10^{-3} S/cm) of a solid electrolyte with the NASICON structure at room temperature was found for the composition $Li_{1.5}Al_{0.4}Cr_{0.1}Ge_{1.5}(PO_4)_3$ [36].

The data on the co-doping of $LiTi_2(PO_4)_3$ with various trivalent cations have been systematized in works [38,123]. It was shown that doping $Li_{1.3}Al_{0.3}Ti_{1.7}(PO_4)_3$ with small gallium cations leads to the replacement of not only titanium ions, but also aluminum, while doping with more bulky yttrium and scandium cations leads to the formation of $ScPO_4$ and YPO_4 and their segregation at grain boundaries, resulting in an increase in the density of the obtained ceramics and a decrease in the conductivity due to the blocking of lithium migration pathways. The co-doping of $LiTi_2(PO_4)_3$ with iron and aluminum ions results in a high ionic conductivity (2.2×10^{-3} S/cm at room temperature) [124]. The

ionic conductivity of $Li_{1.3}Al_{0.3-y}B_yTi_{1.7}(PO_4)_3$ electrolytes was shown to increase with the increasing B^{3+} content, reaching a maximum at y = 0.08 (8.3×10^{-4} S/cm) [125]. Among the $Li_{1.3}Al_{0.22-x}B_{0.08}In_xTi_{1.7}(PO_4)_3$ electrolytes, the highest conductivity (1.1×10^{-3} S/cm) was found for the material with x = 0.01, which was caused by its high relative density.

Among the works devoted to co-doping in the cationic and anionic sublattices, it is also worth mentioning reference [126], where the substitution of phosphorus with silicon with the formation of $Li_{1+x+y}Al_xTi_{2-x}Si_yP_{3-y}O_{12}$ led to a significant increase in conductivity by up to 3×10^{-3} S/cm. The main results of the ionic conductivity of the co-doped NASICON materials are shown in Figure 5.
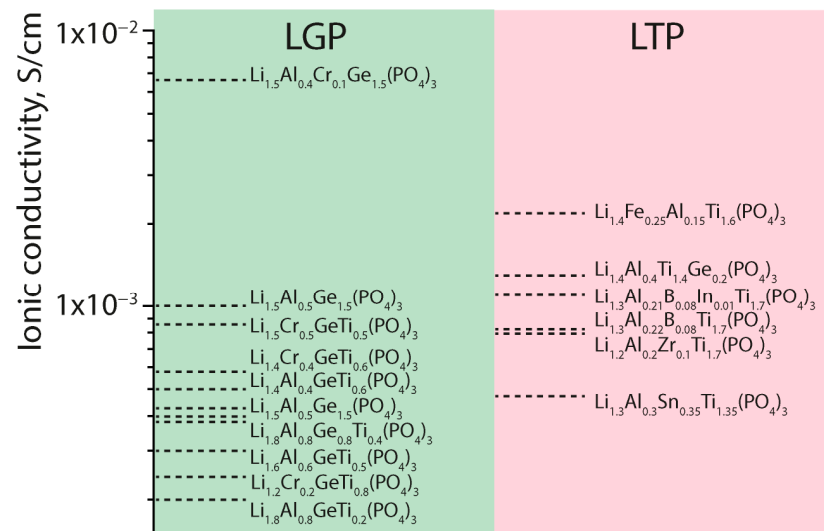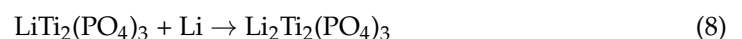

Figure 5. Ionic conductivity of some co-doped lithium NASICON materials. Data taken from [35,36,62,63,113,117,119–122,124,125].

4. Ways to Improve Performance of Lithium Metal Batteries with an Electrolyte Based on NASICON-Structured Phosphates

Figure 6 outlines the main problems of ASSLBs with the NASICON-type electrolytes and ways of overcoming them. The use of LATP- and LAGP-based electrolytes in ASSLBs is associated with several problems, including a high resistance of the electrode/electrolyte interface, a chemical interaction of electrolytes with lithium metal, and dendrite formation. Poor contact at the solid electrolyte/lithium interface or the solid electrolyte/cathode interface hinders battery performance due to high resistance and slows the diffusion of lithium ions. Additionally, materials based on lithium titanium and lithium germanium phosphates can be reduced by lithium anode [127–129]. Products formed by reactions (7) and (8) have undesirable electronic conductivity [118].

$$2LiGe_2(PO_4)_3 + 4Li \rightarrow 3GeO_2 + 6LiPO_3 + Ge \qquad (7)$$

$$LiTi_2(PO_4)_3 + Li \rightarrow Li_2Ti_2(PO_4)_3 \qquad (8)$$
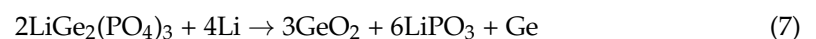
Figure 6. The main challenges of electrolyte and electrolyte/electrode interfaces in ASSLBs. Electrolyte and electrolyte/electrode interfaces are shaded in blue, the main challenges are in pink, and ways to overcome them are in green.
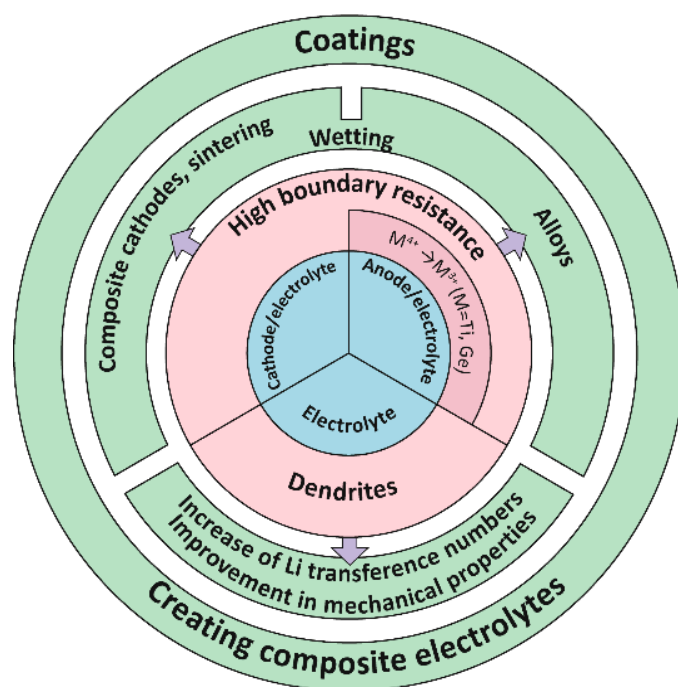
An important issue in lithium metal batteries is dendrite formation. However, it is worth noting that for ASSLBs, this risk is minimal, and dendrite formation can only occur in the electrolyte microcavities. As mentioned in the works [130–132], the main cause of dendrite growth in ceramic electrolytes is their electronic conductivity, which is higher at areas of defects, surface impurities, gaps, and grain boundaries. Thus, the suppression of the chemical reaction between an electrolyte and lithium anode that leads to the formation of an electron-conducting layer can also reduce the risk of dendrite growth through an electrolyte.

Composite cathodes, lithium alloys, coating solid electrolytes or lithium anodes, wetting by liquid electrolytes, and creating composite electrolytes containing a polymer are used to solve the aforementioned problems (Figure 6).

4.1. Coating

The most common approach used to solve the issues described above is to create a thin protective layer of inorganic materials [133–135] or polymers [136–139] on the solid electrolyte surface. Their coating on the electrolyte surface can prevent the reduction of titanium or germanium cations, prevent the formation of lithium dendrites, and stabilize the lithium metal/solid electrolyte interface in ASSLBs [129,140]. Over the past decades, many artificial layers have been proposed to inhibit a side reaction at the interface, such as ZnO [141,142], Al_2O_3 [143], AlF_3 [144], BN [145], carbon-based materials [146,147], etc. For example, depositing a 5 nm thick ZnO layer on LATP using atomic layer deposition reduces the overvoltage of a symmetric Li | LATP-modified by ZnO | Li cell compared to an unmodified LATP-based cell. A symmetric Li | LATP-modified by ZnO | Li cells, in contrast to the unmodified electrolyte, exhibits stable cycling for over 500 h. A full $LiFePO_4$ | LATP-modified by ZnO | Li cell showed a reversible capacity of 156 mAh/g for 50 cycles and good capacity retention (98.8% after 50 cycles) [141]. A layer of reduced graphene oxide (rGO) with ZnO at the interface between LAGP and lithium reduced the surface resistance from 1850 (for uncoated LAGP) to 32 Ohm [142]. As a result, the symmetric Li | LAGP modified by rGO with the ZnO | Li cell showed stable cycling for over 800 cycles at 0.15 mA/cm². Liu et al. coated LATP with graphene, resulting in a Li | Gr@LATP | $LiFePO_4$ cell capacity

of 136 mAh/g after 200 cycles at 0.1 mA/cm^2, corresponding to a capacity retention of 86.1% [147].

Based on the analysis of the thermodynamic, chemical, electrochemical stability, and electronic structure, Li et al. [134] proposed seven Li-containing materials (LiCs$_2$VO$_4$, LiRb$_2$VO$_4$, LiRbMoO$_4$, LiCsYO$_6$, LiNa$_3$WO$_5$, Li$_3$TaO$_4$, and LiScO$_2$) as a protective layer for LiTi$_2$(PO$_4$)$_3$. According to the calculations, the electron transfer from lithium metal to solid electrolyte can be successfully blocked by the protective layer to inhibit the dendrite growth [134]. Solid polymer-in-ceramic electrolyte PVDF/LTFSI/Li$_{1.3}$Al$_{0.3}$Ti$_{1.7}$(PO$_4$)$_3$ with the addition of g-C$_3$N$_4$ nanosheets (5 wt% LATP) had a high conductivity of 5.9×10^{-4} S/cm at 25 °C and a lithium transference number of 0.63. However, the capacity and the cycling of the LiNi$_{0.8}$Co$_{0.1}$Mn$_{0.1}$O$_2$ | Li cell with obtained electrolytes were not satisfactory due to titanium reduction when in contact with lithium. The addition of a thin layer of a similar composition without LATP in the cell between the electrolyte and lithium significantly improved the electrochemical performance. The discharge capacity was 170.1 mAh/g at the first cycle with an 88% retention after 120 charge/discharge cycles at 0.2C, with a Coulomb efficiency of 99% [148]. Some of the results obtained on the reduction of electrode/electrolyte boundary resistance by introducing a protective layer are shown in Table 1.

Table 1. Data on the reduction of the electrode/electrolyte boundary resistance by introducing a protective layer.

Electrolyte	Protective Layer	Ionic Conductivity and Activation Energy	Resistance of the Electrode/Electrolyte	Ref.
LAGP Li$_{1.5}$Al$_{0.5}$Ge$_{1.5}$(PO$_4$)$_3$	LiPON layer on the lithium anode	0.16 S/cm, Ea = 0.266 eV	Surface resistance decreased from 617 to 289 Ohm	[149]
LAGP Li$_{1.5}$Al$_{0.5}$Ge$_{0.5}$(PO$_4$)$_3$	Reduced graphene oxide layer with ZnO at the boundary between LAGP electrolyte and metallic Li	0.32 S/cm	Surface resistance decreased from 1840 to 32 Ohm	[142]
LAGP Li$_{1.5}$Al$_{0.5}$Ge$_{1.5}$(PO$_4$)$_3$	Introduction of a LiF@Li-Zn layer at the LAGP/Li interface	2.5×10^{-4} S/cm, Ea = 0.24 eV	Surface resistance was 420 Ohm/cm^2	[150]
LAGP Li$_{1.5}$Al$_{0.5}$Ge$_{1.5}$(PO$_4$)$_3$	Polymer coatings containing GDLA-UAG layer and fluoroethylene carbonate, LiTFSI, and PEGMEMA	4.8×10^{-4} S/cm, Ea = 0.31 eV	Surface resistance decreased from 20 kOhm to 190 Ohm	[151]
LATP Li$_{1.3}$Al$_{0.3}$Ti$_{1.7}$(PO$_4$)$_3$	Addition of a liquid electrolyte to LATP electrolyte and a layer containing PVDF and LiTFSI	—	Surface resistance decreased from 1000 to 125 Ohm.	[152]
LATP Li$_{1.3}$Al$_{0.3}$Ti$_{1.7}$(PO$_4$)$_3$	Addition of 15% liquid electrolyte	—	Surface resistance decreased from ~5000 Ohm to ~100 Ohm (after 25 h of contact with lithium metal)	[153]
LATP Li$_{1.3}$Al$_{0.3}$Ti$_{1.7}$(PO$_4$)$_3$	ZnO layer deposition using ALD method	1.7×10^{-4} S/cm	The total resistance of the Li	Li cell decreased from 20 kOhm to 2.7 kOhm	[141]

Coatings are used on both the anodic and cathodic sides of solid electrolytes to reduce the resistance and to create a more stable interface [154,155]. For example, the coating of the surface of the Li$_{1.3}$Al$_{0.3}$Ti$_{1.7}$(PO$_4$)$_3$ solid electrolyte with various functional polymers was described. A protective layer of poly(vinylene carbonate) + tetraglyme was applied on the LATP/LiFePO$_4$ interface, and a protective layer of poly(vinylidene fluoride-co-hexafluoropropylene) (PVDF-HFP) + tetraglyme was applied to the surface of the LATP

facing the lithium anode. The cathodic layer reduced the resistance at the LATP/LiFePO$_4$ interface, and the anodic layer protected the LATP from reduction [156]. This cell showed a low interfacial resistance, excellent cycling stability ($\sim$90% retention after 300 cycles), and stable cycling for 3000 h at 60 °C. The application of a thin layer of LiNbO$_3$ to the LiNi$_{0.6}$Co$_{0.2}$Mn$_{0.2}$O$_2$ cathode led to a slight decrease in the initial discharge capacity due to the overcoming of the additional layer of lithium cations, but contributed to a more stable interface between the LiNi$_{0.6}$Co$_{0.2}$Mn$_{0.2}$O$_2$ and composite polymer electrolyte based on a polymer mixture of polysulfonamine-PVDF-HFP and LATP nanoparticles with a modified 3-aminopropyltriethoxysilane surface that promoted the maintenance of a high cycling capacity [157].

4.2. Addition of a Liquid Electrolyte

A common approach used to improve lithium metal batteries with solid-state electrolytes is the use of hybrid "solid-liquid" or "gel" interlayers, in which the electrode/electrolyte impedance can be significantly reduced as a result of the improved wetting of interfaces [148,158–163]. For example, the addition of 15% liquid electrolyte to the LATP leads to a decrease in the Li/electrolyte interface resistance from ~5000 Ohm to ~100 Ohm (after 25 h of contact with lithium metal) [153]. The addition of a liquid electrolyte to an ASSLB with a LATP electrolyte and an interlayer containing PVDF and LiTFSI led to a decrease in resistance at the Li/electrolyte interface from 1000 to 125 Ohm, and the LiFePO$_4$ | Li cell showed a discharge capacity of 150 mAh/g with a 96% retention after 250 cycles [152]. Ionic liquids can also be used as a "gel" interlayer [164,165]. The interfacial resistance of the anode/electrolyte interface can also be significantly reduced by using lithium-based alloys with small amounts of various metal additives [166–168]. Pressing and sintering layers of electrode material and solid electrolyte at high temperatures are also used to reduce the resistance at the solid electrolyte/cathode interface [169,170].

It is worth noting that a drop of liquid electrolyte is sufficient to improve the electrode/solid electrolyte interface, which significantly reduces the boundary resistance, forms a protective interfacial solid–liquid electrolyte interphase, preventing the reduction of LATP by Li metal, and increases the battery durability [148,152,162,171]. Batteries with a higher amount of liquid electrolytes are referred to as hybrid solid–liquid lithium metal batteries [172]. According to numerous analytical studies, it is most likely that "intermediate" hybrid solid–liquid batteries will be commercialized in the medium term, using liquid electrolytes at least for cathode wetting. In this case, cathode materials should have sufficient porosity to be wetted with liquid electrolytes, and the proportion of liquid electrolytes will be 20–30% of the cathode volume [173,174].

4.3. Creation of Composite Electrolytes Containing Polymer and Inorganic Phases

One of the problems limiting the commercialization of ASSLBs with NASICON-type electrolytes is the difficulty of producing thin films and their limited flexibility. Typical electrode assembly techniques (winding, Z-folding, stacking) are limited to stacking techniques that do not require sheet bending [173,174]. As a result, cell stacking and the assembly of ASSLBs are technically challenging. The use of composite polymer–inorganic solid electrolytes is the most promising way to overcome this problem from this point of view.

Polymer–inorganic composites are dispersions of various kinds of additives in a polymer matrix. Their advantages include an increased ionic conductivity, mechanical strength, thermal stability, and stability of the electrode/electrolyte interface compared to polymeric or inorganic electrolytes alone [175].

An increase in the ionic conductivity in composites can also be explained by the interaction at the interface. This phenomenon was first described by Liang for a system characterized by high ionic conductivity and consisting of low-conductive LiI and dielectric Al$_2$O$_3$ [176].

Later, an explanation of this phenomenon was proposed by Maier [177]. According to his theory, one kind of ion forming the salt is predominantly sorbed on the oxide

surface, to which a high concentration of defects is realized in a thin Debye layer, ensuring the formation of a highly conductive layer (see also Section 2). Similarly, the carrier concentration at the interface of inorganic nanoparticles embedded in polymers can increase. The presence of many electronegative atoms on the surface of oxygen-containing dopant particles creates favorable conditions for the sorption and transfer of cations, providing an improvement of transport processes. In addition, polymer packing is deformed near the nanoparticle surface, polymer chains are disordered, and a free volume is created. At high concentrations of inorganic particles, surface layers can form percolation structures through which cations are transported [178].

Composite electrolytes most often consist of a polymer matrix, an inorganic filler, and a low-molecular-weight lithium salt dissolved in the polymer matrix. The electrochemical characteristics of the resulting composites depend primarily on the polymer type, additives, their amount and dispersity, as well as the method of composite production [179–181]. In general, polymer–ceramic composite electrolytes can be divided into the following two main groups: ceramic-in-polymer composites (CIP) and polymer-in-ceramic composites (PIC) (Figure 7).
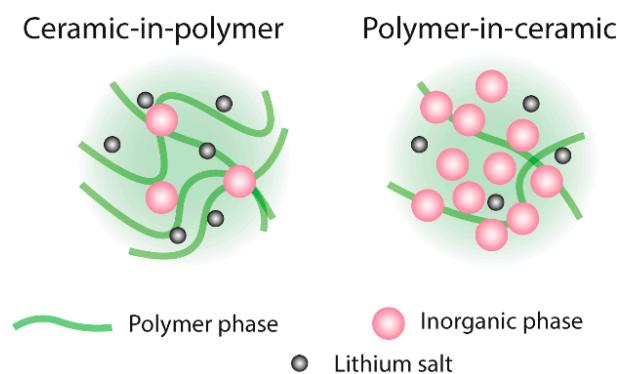

Figure 7. Schematic representation of ceramic-in-polymer and polymer-in-ceramic composite electrolytes.

CIP composites are characterized by high flexibility and a low cost, while PIC composites are characterized by high mechanical strength and safety. According to the polymer matrix type, composites can be divided into systems based on inert polymers with dissolved salt (polymer/salt) and systems containing cation-exchange membranes. A common approach is the use of "solid-liquid" hybrid electrolytes in which the electrode/electrolyte contact impedance can be significantly reduced as a result of the improved wetting of the interface [163,182].

Composite electrolytes are mainly prepared using a casting technique involving the dispersion of inorganic particles and the dissolution of a low-molecular-weight lithium salt in a polymer solution followed by casting, drying, and pressing to produce a solid conductive film [159,160,183–186]. Solution casting is a conventional technique used for manufacturing polymer composite/ceramic electrolyte membranes with thicknesses ranging from 50 to 300 μm. A wide range of CPEs are developed using this method with different concentrations of fillers, salt, and polymer. Alternative methods for preparing composite electrolytes are electrospinning [161,187] and mechanochemical synthesis based on the co-grinding of ceramic and polymer followed by pressing to obtain a conductive film [188,189].

4.3.1. Composite Electrolytes Containing Nonconductive Polymers

Composite electrolytes with nonconductive polymers usually contain lithium salts, such as lithium perchlorate, trifluorosulfonylimide, hexafluorophosphate, etc. It is necessary to use polymers containing electronegative atoms to dissolve lithium salts completely. Therefore, PEO, polypropylene oxide, polyacrylonitrile, PVDF, PVF-HFP, polycaprolactone,

etc., are the most common inert polymer matrices for composite electrolytes [127,179,190]. It should be noted that the use of such polymers also favors the formation of cationic defects at the interfaces with the solid electrolyte, which causes an increase in the ionic conductivity of the system. In recent years, fluorine-containing polymers have attracted a special attention [191].

Both inert inorganic materials that do not directly participate in ionic transport—alumina and silica [192–194]—and ones that are characterized by their own conductivity, such as solid electrolytes with lithium conductivity, i.e., garnets, lithium titanium, or germanium phosphates with the NASICON structure [159–161,184–186,195], and carbon materials [196], are used as additives. The latter attracts attention primarily because of the possibility of increasing the mechanical strength of the resulting composites. To prevent the appearance of electronic conductivity and short circuits, Tang et al. [197] applied a layer of insulating clay material to the carbon nanotubes. With the introduction of only 5% of the additive, the tensile strength of the composite increased by more than 160%. Reducing the particle size and, consequently, increasing the surface area leads to an increase in the extent of interfaces and ionic conductivity of the obtained system. The maximum effect is achieved with the addition of nanosized particles [191]. The addition of inorganic particles to polymer/salt electrolytes leads to a certain increase in the lithium transference numbers; the values most often range from 0.4 to 0.7 depending on the nature of the particles, salt, and polymer matrix [198].

When "active" particles such as NASICON phosphates are added to polymer/salt electrolytes, cations can be transferred in both the polymer with dissolved salt and through the inorganic dopant. It can be assumed that the interface polymer/salt and the inorganic dopant contribute the most to the conductivity increase [182,199]. Most authors attribute an increase in the conductivity to a decrease in the polymer crystallinity [199], an increased mobility of charge carriers at the interface between the polymer/salt and the inorganic dopant [200], and an increase in the degree of dissociation of the salt dissolved in the polymer as a result of an acid–base interaction with dopant particles, which increases the concentration of the charge carriers [201]. Data on the local environment and dynamics of lithium ions in composite electrolytes can be obtained via solid-state Li nuclear magnetic resonance (NMR) [202–204]. The relatively spatial arrangement of different Li components can be investigated using two-dimensional NMR ^{7}Li exchange spectroscopy (2D NMR EXSY) [205]. For example, the ^{7}Li 2D EXSY NMR of the cubic $Li_7La_3Zr_2O_{12}$-PEO-$LiClO_4$) composite reveals peaks from $LiClO_4$ dissolved in PEO, Li in LLZO, and Li located at the polymer–inorganic interface. It is shown that there is a spin exchange between the $LiClO_4$ in PEO and the interfacial Li [202]. NMR EXSY has proven to be a powerful tool to study both the lithium exchange between the polymer matrix and solid electrolyte and the lithium-ion pathways in composite electrolytes [199,202,206,207]. Yan et al. showed a high rate of lithium transfer via three-dimensional porous LATP and polymer electrolyte/LATP interface using solid state NMR [208].

For ceramic-in-polymer electrolytes, the maximum conductivity was obtained at a relatively low content of NASICON phosphates (5–20 wt%) [185,209,210]. Han et al. reported the maximum conductivity (2.3×10^{-4} S/cm at room temperature) for the composite electrolyte containing 10 wt% $Li_3Zr_2Si_2PO_{12}$ and PVDF/LiTFSI [185]. The resulting PVDF/LiTFSI/$Li_3Zr_2Si_2PO_{12}$ electrolyte was characterized by a wide electrochemical stability window (>5.2 V vs. Li^+/Li), sufficient mechanical strength, and excellent stability against lithium metal. The $LiNi_{0.5}Co_{0.2}Mn_{0.3}O_2$ | PVDF/LiTFSI/$Li_3Zr_2Si_2PO_{12}$ | Li battery cell showed an initial discharge capacity of ~170 mAh/g at 0.1 C with a Coulomb efficiency of 99%, and retained an 88.5% capacity after 100 charge/discharge cycles (Figure 8). He et al. prepared a solid-state composite electrolyte based on $Li_{1.4}Al_{0.4}Ti_{1.6}(PO_4)_3$ (LATP), PEO, LiTFSI, and 3,3′,4,4′-diphenyltetracarboxyl dianhydride-4,4′-oxidianiline [209]. The best electrochemical characteristics were obtained for the 15% ratio of LATP to PEO. LATP reduces the crystallinity of PEO and increases its ionic conductivity. A nanofiber membrane based on 3,3′,4,4′-diphenyltetracarboxylic acid dianhydride-4,4′-oxydianiline polyimide (PI)

showed an increased thermal stability, and a symmetrical Li | Li cell with an obtained electrolyte was stable for 1000 h at a current density of 0.5 mA/cm^2. The LiNi$_{0.8}$Co$_{0.1}$Mn$_{0.1}$O$_2$ | Li battery cell retained 95% capacity after 100 cycles at 0.2 C (170.7 mAh/g) with a Coulomb efficiency of ~100% (Figure 8).

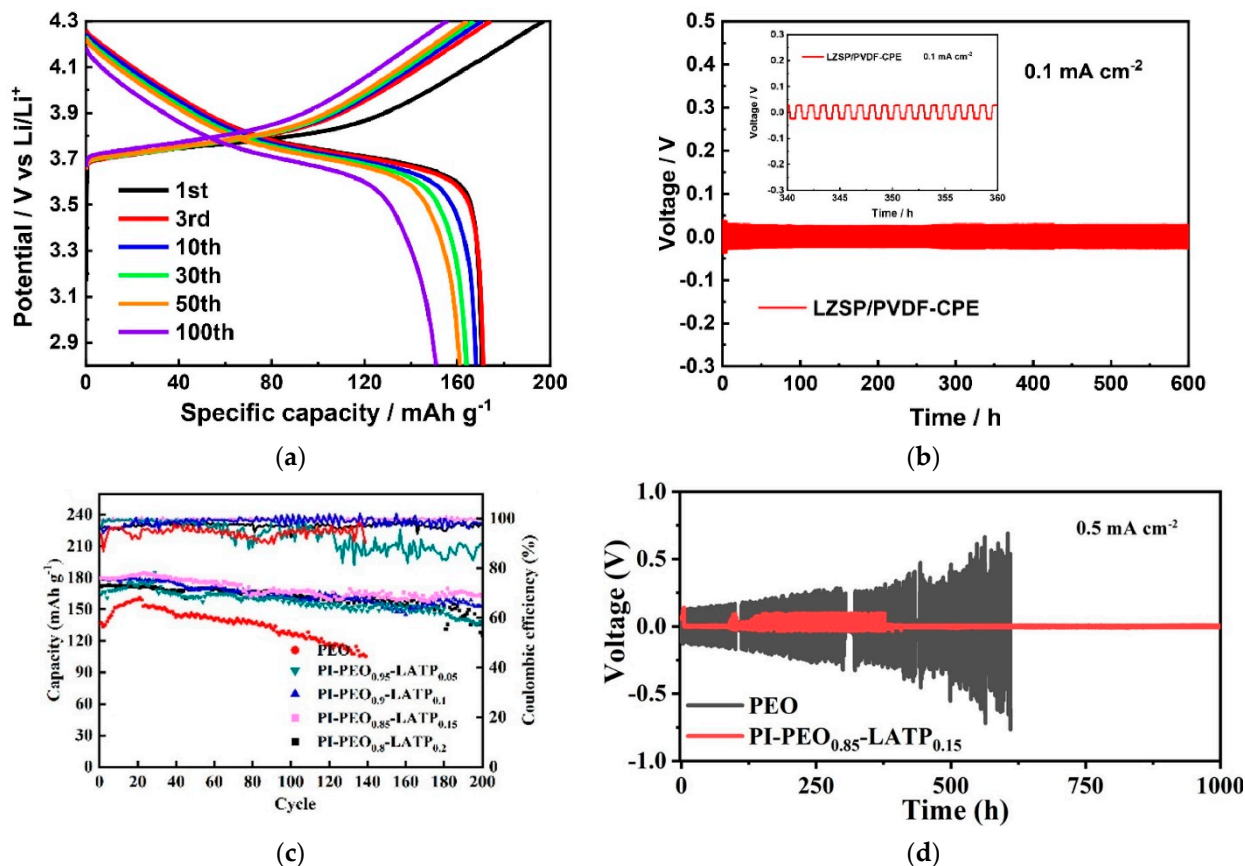**Figure 8.** Stability of electrolytes against lithium and the cycling performance of lithium metal batteries with (**a**,**b**) PVDF/LiTFSI/Li$_3$Zr$_2$Si$_2$PO$_{12}$ composite polymer electrolytes (LiNi$_{0.5}$Co$_{0.2}$Mn$_{0.3}$O$_2$ cathode) [185]; (**c**,**d**) PEO-PI/LiTFSI/Li$_{1.4}$Al$_{0.4}$Ti$_{1.6}$(PO$_4$)$_3$ composite polymer electrolytes with the different Li$_{1.4}$Al$_{0.4}$Ti$_{1.6}$(PO$_4$)$_3$ content (LiNi$_{0.8}$Co$_{0.1}$Mn$_{0.1}$O$_2$ cathode) [209].

It is worth noting that the addition of inorganic particles to polymers significantly increases the electrochemical stability window of electrolytes, as shown in references [185,209] (Figure 9a,b). The electrochemical stability window is also influenced by the shape of introduced particles. For example, the electrochemical stability window of a PEO/LiTFSI/Li$_{1.3}$Al$_{0.3}$Ti$_{1.7}$(PO$_4$)$_3$-based composite electrolyte is 4.62 V, and 4.75 V when 30 wt.% of particulate synthesized LATP and hollow sphere LATP are introduced, respectively (Figure 9c) [210].
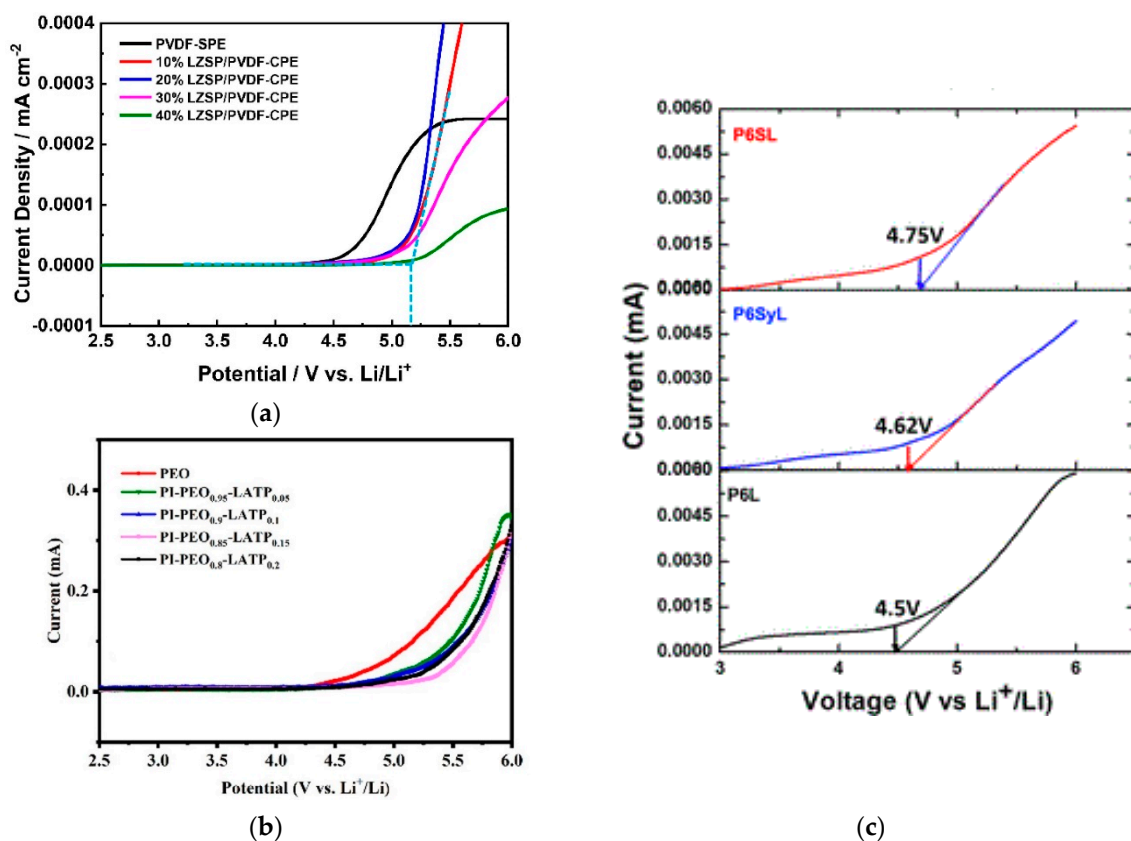
Figure 9. Linear sweep voltammetry of (**a**) PVDF/LiTFSI/$Li_3Zr_2Si_2PO_{12}$ composite polymer electrolytes [185]; (**b**) PEO-PI/LiTFSI/$Li_{1.4}Al_{0.4}Ti_{1.6}(PO_4)_3$ composite polymer electrolytes with the different $Li_{1.4}Al_{0.4}Ti_{1.6}(PO_4)_3$ content [209]; (**c**) PEO/LiTFSI (P6L), PEO/LiTFSI/particulate synthesized $Li_{1.3}Al_{0.3}Ti_{1.7}(PO_4)_3$ (P6SyL) and PEO/LiTFSI/hollow spheres $Li_{1.3}Al_{0.3}Ti_{1.7}(PO_4)_3$ (P6SL) [210].

Polymer-in-ceramic electrolytes seem even more attractive. The reason for this is their improved mechanical properties, thermal stability, and resistance to the metal anode [148,183,210–212]. In some cases, increasing the dopant content increases the lithium transference numbers by reducing the anion mobility as a result of the interactions with the dopant surface [210]. There are discrepancies in the content of the inorganic phase in the composite, according to which its type is determined—"ceramics-in-polymer" or "polymer-in-ceramics". An increase in the elasticity modulus is noted at the inorganic phase content of 20–30 wt.% [212]. According to reference [213], the term "polymer-in-ceramics" is reported for a phosphate content of 30 wt%. Chen et al. [214] classified composites with a 50 wt% of inorganic particles to the intermediate type, and classified composites with >80 wt% of inorganic particles to "polymer-in-ceramics". The classification is more often carried out according to which of the components (polymer or ceramics) is predominant [183].

The influence of the shape and spatial orientation of the inorganic particles should also be noted. The use of nanofibers, nanoplates, nanotubes, or 3D porous structures as dopants promotes the creation of extended ion transport pathways and makes it possible to obtain materials with a high conductivity [178]. For example, the conductivity of a PEO/polyethylene glycol/$LiClO_4$/LATP (40 vol%) electrolyte with NASICON phosphates connected to each other and oriented perpendicularly to the electrolyte plane reaches 5.2×10^{-5} S/cm at room temperature, which is 3.6 times higher than the composite with LATP particles randomly distributed in the electrolyte [184]. Patil et al. reported a composite electrolyte based on PEO, LiTFSI, and $Li_{1.3}Al_{0.3}Ti_{1.7}(PO_4)_3$ filler (30 wt%) [210]. The composites with a random distribution of LATP particles (200 nm) and with primary particles arranged in hollow LATP spheres (7–15 μm) are superior to the unmodified PEO/LiTFSI electrolyte in terms of mechanical, conductive, and electrochemical charac-

teristics. The conductivity of the composite with LATP spheres was 1.6×10^{-4} S/cm (25 °C) [210]. Furthermore, the resulting composite was characterized by a higher lithium transference number. The electrochemical characterization of symmetrical Li | Li cells with PEO/LiTFSI/LATP spheres electrolytes showed less overvoltage and stable operation during 500 h of cycling at a current density of 0.1 mA/cm^2. This illustrates the promise of works regarding the development of particle microstructures in the case of composite polymer electrolytes.

4.3.2. Composite Electrolytes with Cation-Exchange Membranes

Cation-exchange membranes are a promising class of polymer electrolytes, so-called single-ion conductors [178,210–217]. The anions in these materials are covalently bound to the polymer matrix, and thus, such electrolytes have only cationic conductivity. The lack of anion mobility prevents dendrite formation during the cycling of batteries with lithium metal anode. Functional groups are usually located on the side branches of the main polymer chain to maximize cation mobility. Recent works in the development of single-ion conductors for battery applications has been dominated by cation-exchange membranes containing the functional sulfonylimide groups $R\text{-}SO_2N^{(-)}SO_2\text{-}X$, since their bulk conjugated structure can effectively delocalize the negative charge [63–66,218–223]. These functional groups reduce the dissociation energy with Li$^+$ cations due to the high delocalization of the negative charge in the anions, facilitating ionic transport. The negative charge distribution in $R\text{-}SO_2N^{(-)}SO_2\text{-}X$ can be further improved by introducing various bulk electronegative groups such as -CF$_3$, -Ph, or -PhCF$_3$ [67–70]. The solvation of such membranes with organic aprotic solvents provides high values of ionic conductivity, which can reach values of up to 10^{-4}–10^{-3} S/cm at room temperature [178,221,224]. The number of works on the creation of composite polymer electrolytes based on cation-exchange membranes and NASICON phosphates (active inorganic ceramic particles) for their application in lithium metal batteries is limited, while the addition of inorganic particles contributes to the suppression of dendrite growth [157,158]. Yu et al. reported that they obtained a polymer-in-ceramic composite electrolyte based on $Li_{1.3}Al_{0.3}Ti_{1.7}(PO_4)_3$ (LATP), cross-linked poly[bis(2-(2-methoxyethoxy)ethoxy)-phosphazene], and (4-styrenesulfonyl)-(trifluoromethanesulfonyl)lithium imide (LiSTFSI) with a ~4:1 volume ratio of LATP to polymer solution [158]. After the addition of ethylene carbonate and dimethyl carbonate plasticizer (EC-DMC, 1:1, vol./vol, ~150 wt% in terms of polymer), composite electrolytes with a high ionic conductivity of 3.1×10^{-4} S/cm at room temperature, a wide electrochemical stability window of 5 V, and lithium transference numbers of 0.94 were obtained. The Li | LiFePO$_4$ battery exhibited stable cycling with an initial discharge capacity of 131.8 mAh/g, and maintained a capacity of 122.7 mAh/g after 500 cycles at 0.5 C.

Some research papers report the addition of a small amount of plasticizer or liquid electrolyte to the battery cell to increase the electrolyte conductivity and improve the ionic transport at the electrode/electrolyte interface [158–161]. An example of the use of such "solid-liquid" hybrid electrolytes is a lithium–air battery cell with an electrolyte based on a copolymer of PVDF-HFP, LTFSI, and LATP (50 wt% in terms of polymer) with a small amount of 1M LTFSI solution in tetraglyme [160]. The composite electrolyte of the LATP/PVDF composition (mass ratio LATP: PVDF = 0:1, 1:1, 2:1, and 3:1) was kept in 1M of LiPF$_6$ solution in a mixture of EC—DMC—ethyl methyl carbonate (1:1:1 by volume). The highest liquid electrolyte absorption and conductivity (9.67×10^{-4} S/cm) was observed for LATP:PVDF = 2:1. The Li | LiFePO$_4$ battery cell with this electrolyte showed a discharge capacity of 163.5 mAh/g at 0.1 C, with a 91% capacity retention after 50 cycles. The characteristics obtained for the cell with the composite electrolyte with the addition of LATP exceeded the values for the cell with the PVDF-based electrolyte (113 mAh/g at 0.1 C with 91% capacity retention after 50 cycles) [159]. Overhoff et al. prepared a composite ceramic-in-polymer electrolyte based on a mixture of polysulfonamine-PVDF-HFP and LATP nanoparticles with a surface modified with 3-aminopropyltriethoxysilane [157]. The obtained material was plasticized via an EC-propylene carbonate mixture (38 wt% swelling).

The conductivity of the resulting electrolyte with a 20 wt% of LATP was 7×10^{-4} S/cm at 40 °C.

The addition of a small amount of polyelectrolyte to the cathode material to fill the gaps between the inorganic particles aims to increase the intergrain's ionic conductivity [225]. For example, the use of a Nafion solution as a binder for the cathode material when using a solid electrolyte with the NASICON structure was described in ref. [226]. The addition of a polymer electrolyte to the cathode material not only binds its particles, but also allows for ion transport within the cathode material and at the cathode/electrolyte interface. In some studies, lithium salts were added to cathode materials along with an active material and binder [148,185,210].

5. Conclusions

Currently, lithium-ion batteries with liquid electrolytes dominate among rechargeable batteries. However, there are severe issues with their safety (the probability of electrolyte leakage, growth of lithium dendrites caused by contact of anode with liquid electrolytes, and the electrolyte evaporation at elevated temperatures). The development of solid electrolytes with a conductivity of $>10^{-3}$ S/cm at room temperature and a wide electrochemical stability window (>5 V vs. Li/Li$^+$) is one possible way to solve these problems and can allow for the creation of ASSLBs that can be used over a wide temperature range.

In this review, some of the most promising materials for ASSLBs with NASICON-structured phosphates as electrolytes with a high ionic conductivity, favorable physical and chemical stabilities, and a low cost are discussed, focusing on the works published in the past few years. The results of the studies on NASICON-structured phosphates and their composites of various types with polymeric materials are presented. Various approaches for increasing the ionic conductivity and solving problems arising from their use as electrolytes in batteries, including the challenge of the electrolyte/electrode interface, are discussed. Co-doping, which can increase the ionic conductivity to 6.6×10^{-3} S/cm at room temperature, is considered among other methods of increasing the ionic conductivity of electrolytes. The coating of various materials, including polymeric and inorganic ones, to the surface of the electrolyte or electrode can significantly suppress side reactions and reduce resistance at the electrode–solid electrolyte interface. It is worth mentioning the works of cycling electrochemical cells with phosphate-based electrolytes with the NASICON structure and lithium metal, which operate stably at room temperature and over 100 cycles, indicating that significant progress has been made in solving the problems of relatively low conductivity, low chemical stability, and dendrite formation.

Despite significant progress in the field of ASSLBs with the NASICON-type electrolytes, their commercialization is still hampered by several problems, including the insufficient mechanical strength of the electrolytes, and interphase instability, especially of the lithium titanium phosphates towards the lithium metal anode. It appears that the use of a synergistic approach involving the creation of composites and the introduction of additives into the electrolyte can help to achieve the goals of increasing the interfacial stability and reducing the grain boundary resistance.

The replacement of liquid electrolytes by solid ones seems to be necessary and inevitable for many devices, and composite polymer electrolytes, especially those containing a cation-conducting polymer matrix and inorganic fillers, have the best prospects for real applications due to their excellent complex properties among all electrolytes. However, the study of the properties and applications of such composite polymer electrolytes in lithium batteries is still at an early stage. Therefore, it can be assumed that the development of new cation-exchange polymer materials and new inorganic ionic conductors will be the most promising. In this case, the optimization of the ratio of organic and inorganic components in composite electrolytes, the size, the spatial organization, and the content of inorganic fillers can significantly improve ion transport in composite polymer electrolytes. It is worth paying attention to the use of modern research methods and numerical modeling to establish the mechanisms of lithium-ion transport in composite materials.

References

1.　Li, J.; Kong, Z.; Liu, X.; Zheng, B.; Fan, Q.H.; Garratt, E.; Schuelke, T.; Wang, K.; Xu, H.; Jin, H. Strategies to Anode Protection in Lithium Metal Battery: A Review. *InfoMat* **2021**, *3*, 1333–1363. [CrossRef]

2.　Pang, M.-C.; Wei, Y.; Wang, H.; Marinescu, M.; Yan, Y.; Offer, G.J. Large-Format Bipolar and Parallel Solid-State Lithium-Metal Cell Stacks: A Thermally Coupled Model-Based Comparative Study. *J. Electrochem. Soc.* **2020**, *167*, 160555. [CrossRef]

3.　Cao, D.; Sun, X.; Wang, Y.; Zhu, H. Bipolar Stackings High Voltage and High Cell Level Energy Density Sulfide Based All-Solid-State Batteries. *Energy Storage Mater.* **2022**, *48*, 458–465. [CrossRef]

4.　Braga, M.H.; Subramaniyam, C.M.; Murchison, A.J.; Goodenough, J.B. Nontraditional, Safe, High Voltage Rechargeable Cells of Long Cycle Life. *J. Am. Chem. Soc.* **2018**, *140*, 6343–6352. [CrossRef]

5.　Lee, N.; Oh, J.; Choi, J.W. Anode-Less All-Solid-State Batteries: Recent Advances and Future Outlook. *Mater. Futures* **2023**, *2*, 013502. [CrossRef]

6.　Wang, S.; Fang, R.; Li, Y.; Liu, Y.; Xin, C.; Richter, F.H.; Nan, C.-W. Interfacial Challenges for All-Solid-State Batteries Based on Sulfide Solid Electrolytes. *J. Mater.* **2021**, *7*, 209–218. [CrossRef]

7.　Subramanian, K.; Alexander, G.V.; Karthik, K.; Patra, S.; Indu, M.S.; Sreejith, O.V.; Viswanathan, R.; Narayanasamy, J.; Murugan, R. A Brief Review of Recent Advances in Garnet Structured Solid Electrolyte Based Lithium Metal Batteries. *J. Energy Storage* **2021**, *33*, 102157. [CrossRef]

8.　Kim, K.J.; Balaish, M.; Wadaguchi, M.; Kong, L.; Rupp, J.L.M. Solid-State Li–Metal Batteries: Challenges and Horizons of Oxide and Sulfide Solid Electrolytes and Their Interfaces. *Adv. Energy Mater.* **2021**, *11*, 2002689. [CrossRef]

9.　Wang, C.; Liang, J.; Zhao, Y.; Zheng, M.; Li, X.; Sun, X. All-Solid-State Lithium Batteries Enabled by Sulfide Electrolytes: From Fundamental Research to Practical Engineering Design. *Energy Environ. Sci.* **2021**, *14*, 2577–2619. [CrossRef]

10.　Barbosa, J.C.; Gonçalves, R.; Costa, C.M.; Lanceros-Méndez, S. Toward Sustainable Solid Polymer Electrolytes for Lithium-Ion Batteries. *ACS Omega* **2022**, *7*, 14457–14464. [CrossRef]

11.　Yaroslavtsev, A.B.; Stenina, I.A. Complex Phosphates with the NASICON Structure (M_x $A_2(PO_4)_3$). *Russ. J. Inorg. Chem.* **2006**, *51*, S97–S116. [CrossRef]

12.　Ivanov-Shitz, A.K.; Murin, I.V. *Ionics of Solid State*; St. Petersburg University Press: Saint Petersburg, Russia, 2000. (In Russian)

13.　Robertson, A.; West, A.; Ritchie, A. A Review of Crystalline Lithium-Ion Conductors Suitable for High Temperature Battery Applications. *Solid State Ionics* **1997**, *104*, 1–11. [CrossRef]

14.　Stenina, I.A.; Yaroslavtsev, A.B. Nanomaterials for Lithium-Ion Batteries and Hydrogen Energy. *Pure Appl. Chem.* **2017**, *89*, 1185–1194. [CrossRef]

15.　Li, Q.; Chen, J.; Fan, L.; Kong, X.; Lu, Y. Progress in Electrolytes for Rechargeable Li-Based Batteries and Beyond. *Green Energy Environ.* **2016**, *1*, 18–42. [CrossRef]

16.　Zheng, F.; Kotobuki, M.; Song, S.; Lai, M.O.; Lu, L. Review on Solid Electrolytes for All-Solid-State Lithium-Ion Batteries. *J. Power Sources* **2018**, *389*, 198–213. [CrossRef]

17.　Dias, J.A.; Santagneli, S.H.; Messaddeq, Y. Methods for Lithium Ion NASICON Preparation: From Solid-State Synthesis to Highly Conductive Glass-Ceramics. *J. Phys. Chem. C* **2020**, *124*, 26518–26539. [CrossRef]

18.　Hou, M.; Liang, F.; Chen, K.; Dai, Y.; Xue, D. Challenges and Perspectives of NASICON-Type Solid Electrolytes for All-Solid-State Lithium Batteries. *Nanotechnology* **2020**, *31*, 132003. [CrossRef]

19.　Yaroslavtsev, A. Modification of Solid State Proton Conductors. *Solid State Ionics* **2005**, *176*, 2935–2940. [CrossRef]

20.　Stenina, I.A.; Pinus, I.Y.; Yaroslavtsev, A.B.; Kislitsyn, M.N.; Arkhangel'skij, I.V.; Zhuravlev, N.A. Phase Transformations and Cation Mobility in NASICON Lithium Zirconium Double Phosphates $Li_{1+x}Zr_{2-X}M_x(PO_4)_3$ (M = Sc, Y, In, Nb, Ta). *Russ. J. Inorg. Chem.* **2005**, *50*, 906–911.

21.　Pinus, I.Y.; Khoroshilov, A.V.; Gavrichev, K.S.; Tarasov, V.P.; Yaroslavtsev, A.B. On Cationic Mobility in Nasicon Phosphates $LiTi_2(PO_4)_3$ and $Li_{0.9}Ti_{1.9}Nb_{0.1}(PO_4)_3$. *Solid State Ionics* **2012**, *212*, 112–116. [CrossRef]

22.　Lang, B.; Ziebarth, B.; Elsässer, C. Lithium Ion Conduction in $LiTi_2(PO_4)_3$ and Related Compounds Based on the NASICON Structure: A First-Principles Study. *Chem. Mater.* **2015**, *27*, 5040–5048. [CrossRef]

23.　Mutter, D.; Urban, D.F.; Elsässer, C. Computational Analysis of Composition-Structure-Property-Relationships in NZP-Type Materials for Li-Ion Batteries. *J. Appl. Phys.* **2019**, *125*, 215115. [CrossRef]

24.　Yaroslavtsev, A.B. Ion Conductivity of Composite Materials on the Base of Solid Electrolytes and Ion-Exchange Membranes. *Inorg. Mater.* **2012**, *48*, 1193–1209. [CrossRef]

25. Svitan'ko, A.I.; Novikova, S.A.; Stenina, I.A.; Skopets, V.A.; Yaroslavtsev, A.B. Microstructure and Ion Transport in $Li_{1+x}Ti_{2-x}M_x(PO_4)_3$ (M = Cr, Fe, Al) NASICON-Type Materials. *Inorg. Mater.* **2014**, *50*, 273–279. [CrossRef]

26. Schmalzried, H.F.A. Kröger: The Chemistry of Imperfect Crystals, North-Holland Publishing Company-Amsterdam 1964. 1039 Seiten. Preis: Hfl. 110,-. *Ber. Bunsenges.Phys. Chem.* **1964**, *68*, 608. [CrossRef]

27. Lu, X.; Wang, S.; Xiao, R.; Shi, S.; Li, H.; Chen, L. First-Principles Insight into the Structural Fundamental of Super Ionic Conducting in NASICON $MTi_2(PO_4)_3$ (M = Li, Na) Materials for Rechargeable Batteries. *Nano Energy* **2017**, *41*, 626–633. [CrossRef]

28. Maier, J. Point-Defect Thermodynamics and Size Effects. *Solid State Ionics* **2000**, *131*, 13–22. [CrossRef]

29. Uvarov, N.F.; Hairetdinov, E.F. Unusual Transport and Structural Properties of Mechanically Treated Polycrystalline Silver Iodide. *Solid State Ionics* **1997**, *96*, 219–225. [CrossRef]

30. Yaroslavtsev, A.B. Ion Transport in Heterogeneous Solid Systems. *Russ. J. Inorg. Chem.* **2000**, *45*, S249–S267.

31. Jamnik, J.; Habermeier, H.-U.; Maier, J. Information of Ionic Boundary Effects by a Novel Penetration Impedance Technique. *Phys. B Condens. Matter* **1995**, *204*, 57–64. [CrossRef]

32. Tan, Y.T. Model for Surface Diffusion in AgBr. *J. Appl. Phys.* **1975**, *46*, 469–470. [CrossRef]

33. Christmann, K. *Introduction to Surface Physical Chemistry*; Topics in Physical Chemistry; Springer: Berlin/Heidelberg, Germany, 2013; ISBN 9783662080092.

34. Mariappan, C.R. AC Conductivity Scaling Behavior in Grain and Grain Boundary Response Regime of Fast Lithium Ionic Conductors. *Appl. Phys. A* **2014**, *117*, 847–852. [CrossRef]

35. Kunshina, G.B.; Bocharova, I.V.; Ivanenko, V.I. Preparation of the $Li_{1.5}Al_{0.5}Ge_{1.5}(PO_4)_3$ Solid Electrolyte with High Ionic Conductivity. *Inorg. Mater. Appl. Res.* **2017**, *8*, 238–244. [CrossRef]

36. Illbeigi, M.; Fazlali, A.; Kazazi, M.; Mohammadi, A.H. Effect of Simultaneous Addition of Aluminum and Chromium on the Lithium Ionic Conductivity of $LiGe_2(PO_4)_3$ NASICON-Type Glass–Ceramics. *Solid State Ionics* **2016**, *289*, 180–187. [CrossRef]

37. Gan, H.; Zhu, W.; Zhang, L.; Jia, Y. Zr Doped NASICON-Type LATP Glass-Ceramic as a Super-Thin Coating onto Deoxidized Carbon Wrapped CNT-S Cathode for Lithium-Sulphur Battery. *Electrochim. Acta* **2022**, *423*, 140567. [CrossRef]

38. Kothari, D.H.; Kanchan, D.K. Inter-Grain Li+ Conduction in Sc and Y Doped LATP Compounds. *Phys. B Condens. Matter* **2022**, *627*, 413599. [CrossRef]

39. Nakano, K.; Tanibata, N.; Takeda, H.; Kobayashi, R.; Nakayama, M.; Watanabe, N. Molecular Dynamics Simulation of Li-Ion Conduction at Grain Boundaries in NASICON-Type $LiZr_2(PO_4)_3$ Solid Electrolytes. *J. Phys. Chem. C* **2021**, *125*, 23604–23612. [CrossRef]

40. Arbi, K.; Hoelzel, M.; Kuhn, A.; García-Alvarado, F.; Sanz, J. Structural Factors That Enhance Lithium Mobility in Fast-Ion $Li_{1+x}Ti_{2-x}Al_x(PO_4)_3$ ($0 \leq x \leq 0.4$) Conductors Investigated by Neutron Diffraction in the Temperature Range 100–500 K. *Inorg. Chem.* **2013**, *52*, 9290–9296. [CrossRef]

41. Fergus, J.W. Ceramic and Polymeric Solid Electrolytes for Lithium-Ion Batteries. *J. Power Sources* **2010**, *195*, 4554–4569. [CrossRef]

42. Svitan'ko, A.I.; Novikova, S.A.; Safronov, D.V.; Yaroslavtsev, A.B. Cation Mobility in $Li_{1+x}Ti_{2-x}Cr_x(PO_4)_3$ NASICON-Type Phosphates. *Inorg. Mater.* **2011**, *47*, 1391–1395. [CrossRef]

43. Venkateswara Rao, A.; Veeraiah, V.; Prasada Rao, A.V.; Kishore Babu, B.; Kumar, K.V. Influence of Zr4+ Doping on Structural, Spectroscopic and Conductivity Studies of Lithium Titanium Phosphate. *Ceram. Int.* **2014**, *40*, 13911–13916. [CrossRef]

44. Arbi, K.; Rojo, J.M.; Sanz, J. Lithium Mobility in Titanium Based Nasicon $Li_{1+x}Ti_{2-x}Al_x(PO_4)_3$ and $LiTi_{2-x}Zr_x(PO_4)_3$ Materials Followed by NMR and Impedance Spectroscopy. *J. Eur. Ceram. Soc.* **2007**, *27*, 4215–4218. [CrossRef]

45. Kurzina, E.A.; Stenina, I.A.; Dalvi, A.; Yaroslavtsev, A.B. Synthesis and Ionic Conductivity of Lithium Titanium Phosphate-Based Solid Electrolytes. *Inorg. Mater.* **2021**, *57*, 1035–1042. [CrossRef]

46. DeWees, R.; Wang, H. Synthesis and Properties of NaSICON-type LATP and LAGP Solid Electrolytes. *ChemSusChem* **2019**, *12*, 3713–3725. [CrossRef]

47. Kunshina, G.B.; Shichalin, O.O.; Belov, A.A.; Papynov, E.K.; Bocharova, I.V.; Shcherbina, O.B. Properties of $Li_{1.3}Al_{0.3}Ti_{1.7}(PO_4)_3$ Lithium-Conducting Ceramics Synthesized by Spark Plasma Sintering. *Russ. J. Electrochem.* **2023**, *59*, 173–181. [CrossRef]

48. Xiao, W.; Wang, J.; Fan, L.; Zhang, J.; Li, X. Recent Advances in $Li_{1+x}Al_xTi_{2-x}(PO_4)_3$ Solid-State Electrolyte for Safe Lithium Batteries. *Energy Storage Mater.* **2019**, *19*, 379–400. [CrossRef]

49. Yang, K.; Chen, L.; Ma, J.; He, Y.; Kang, F. Progress and Perspective of $Li_{1+x}Al_xTi_{2-x}(PO_4)_3$ Ceramic Electrolyte in Lithium Batteries. *InfoMat* **2021**, *3*, 1195–1217. [CrossRef]

50. Wu, P.; Zhou, W.; Su, X.; Li, J.; Su, M.; Zhou, X.; Sheldon, B.W.; Lu, W. Recent Advances in Conduction Mechanisms, Synthesis Methods, and Improvement Strategies for $Li_{1+x}Al_xTi_{2-x}(PO_4)_3$ Solid Electrolyte for All-Solid-State Lithium Batteries. *Adv. Energy Mater.* **2023**, *13*, 2203440. [CrossRef]

51. Tolganbek, N.; Mentbayeva, A.; Uzakbaiuly, B.; Kanamura, K.; Bakenov, Z. $Li_{1+x}Al_xTi_{2-x}(PO_4)_3$, NASICON-Type Solid Electrolyte Fabrication with Different Methods. *Mater. Today Proc.* **2020**, *25*, 97–100. [CrossRef]

52. Aono, H.; Sugimoto, E.; Sadaoka, Y.; Imanaka, N.; Adachi, G. Ionic Conductivity of Solid Electrolytes Based on Lithium Titanium Phosphate. *J. Electrochem. Soc.* **1990**, *137*, 1023–1027. [CrossRef]

53. Yen, P.-Y.; Lee, M.-L.; Gregory, D.H.; Liu, W.-R. Optimization of Sintering Process on $Li_{1+x}Al_xTi_{2-x}(PO_4)_3$ Solid Electrolytes for All-Solid-State Lithium-Ion Batteries. *Ceram. Int.* **2020**, *46*, 20529–20536. [CrossRef]

54. Kim, K.M.; Shin, D.O.; Lee, Y.-G. Effects of Preparation Conditions on the Ionic Conductivity of Hydrothermally Synthesized $Li_{1+x}Al_xTi_{2-x}(PO_4)_3$ Solid Electrolytes. *Electrochim. Acta* **2015**, *176*, 1364–1373. [CrossRef]

55. Kothari, D.H.; Kanchan, D.K. Effect of Adding Li$_2$O and MgO on Li-Conductivity in NASICON Material. *Phys. B Condens. Matter* **2021**, *600*, 412489. [CrossRef]

56. Kwatek, K.; Ślubowska, W.; Ruiz, C.; Sobrados, I.; Sanz, J.; Garbarczyk, J.E.; Nowiński, J.L. The Mechanism of Enhanced Ionic Conductivity in Li$_{1.3}$Al$_{0.3}$T$_{i1.7}$(PO$_4$)$_3$–(0.75Li$_2$O·0.25B$_2$O$_3$) Composites. *J. Alloys Compd.* **2020**, *838*, 155623. [CrossRef]

57. Kang, J.; Guo, X.; Gu, R.; Tang, Y.; Hao, H.; Lan, Y.; Jin, L.; Wei, X. Effect of Boron-Based Glass Additives on the Ionic Conductivity of Li$_{1.3}$Al$_{0.3}$Ti$_{1.7}$(PO$_4$)$_3$ Solid Electrolyte. *J. Alloys Compd.* **2023**, *941*, 168857. [CrossRef]

58. Luo, Y.; Gao, H.; Zhao, X. Insights into the Sinterability and Electrical Properties of Li$_{1.3}$Al$_{0.3}$Ti$_{1.7}$(PO$_4$)$_3$–(Li$_2$CO$_3$·Bi$_2$O$_3$) Composite Electrolytes. *Ceram. Int.* **2022**, *48*, 8387–8394. [CrossRef]

59. Bai, H.; Hu, J.; Li, X.; Duan, Y.; Shao, F.; Kozawa, T.; Naito, M.; Zhang, J. Influence of LiBO2 Addition on the Microstructure and Lithium-Ion Conductivity of Li$_{1+x}$Al$_x$Ti$_{2-x}$(PO$_4$)$_3$(x = 0.3) Ceramic Electrolyte. *Ceram. Int.* **2018**, *44*, 6558–6563. [CrossRef]

60. Aono, H.; Sugimoto, E.; Sadaoka, Y.; Imanaka, N.; Adachi, G. Electrical Property and Sinterability of LiTi$_2$(PO$_4$)$_3$ Mixed with Lithium Salt (Li$_3$PO$_4$ or Li$_3$BO$_3$). *Solid State Ionics* **1991**, *47*, 257–264. [CrossRef]

61. Aono, H.; Sugimoto, E.; Sadaoka, Y.; Imanaka, N.; Adachi, G. Electrical Properties and Sinterability for Lithium Germanium Phosphate Li$_{1+x}$M$_x$Ge$_{2-x}$(PO$_4$)$_3$, M = Al, Cr, Ga, Fe, Sc, and In Systems. *Bull. Chem. Soc. Jpn.* **1992**, *65*, 2200–2204. [CrossRef]

62. Moshareva, M.A.; Novikova, S.A. Synthesis and Conductivity Study of Solid Electrolytes Li$_{1+x}$Al$_x$Ge$_{2-x}$(PO$_4$)$_3$ (x = 0–0.65). *Russ. J. Inorg. Chem.* **2018**, *63*, 319–323. [CrossRef]

63. Kunshina, G.B.; Bocharova, I.V.; Lokshin, E.P. Synthesis and Conductivity Studies of Li$_{1.5}$Al$_{0.5}$Ge$_{1.5}$(PO$_4$)$_3$ Solid Electrolyte. *Inorg. Mater.* **2016**, *52*, 279–284. [CrossRef]

64. Zhao, E.; Guo, Y.; Xin, Y.; Xu, G. Facile Synthesis and Performance of NASICON Li$_{1+x}$Al$_x$Ge$_{2-x}$(PO$_4$)$_3$ Electrolytes for All Solid State Lithium-Ion Battery. *Solid State Ionics* **2020**, *356*, 115454. [CrossRef]

65. Pershina, S.V.; Il'ina, E.A.; Druzhinin, K.V.; Farlenkov, A.S. Effect of Li$_2$O–Al$_2$O$_3$–GeO$_2$–P$_2$O$_5$ Glass Crystallization on Stability versus Molten Lithium. *J. Non-Cryst. Solids* **2020**, *527*, 119708. [CrossRef]

66. Tatsumisago, M.; Nagao, M.; Hayashi, A. Recent Development of Sulfide Solid Electrolytes and Interfacial Modification for All-Solid-State Rechargeable Lithium Batteries. *J. Asian Ceram. Soc.* **2013**, *1*, 17–25. [CrossRef]

67. He, K.; Zu, C.; Wang, Y.; Han, B.; Yin, X.; Zhao, H.; Liu, Y.; Chen, J. Stability of Lithium Ion Conductor NASICON Structure Glass Ceramic in Acid and Alkaline Aqueous Solution. *Solid State Ionics* **2014**, *254*, 78–81. [CrossRef]

68. Yan, B.; Zhu, Y.; Pan, F.; Liu, J.; Lu, L. Li$_{1.5}$Al$_{0.5}$Ge$_{1.5}$(PO$_4$)$_3$ Li-Ion Conductor Prepared by Melt-Quench and Low Temperature Pressing. *Solid State Ionics* **2015**, *278*, 65–68. [CrossRef]

69. Sudreau, F.; Petit, D.; Boilot, J.P. Dimorphism, Phase Transitions, and Transport Properties in LiZr$_2$(PO$_4$)$_3$. *J. Solid State Chem.* **1989**, *83*, 78–90. [CrossRef]

70. Stenina, I.A.; Kislitsyn, M.N.; Pinus, I.Y.; Haile, S.M.; Yaroslavtsev, A.B. Phase Transitions and Ion Conductivity in NASICON-Type Compounds Li$_{1\pm X}$Zr$_{2-X}$M$_X$(PO$_4$)$_3$, M = Ta, Nb, Y, Sc, In. *Defect Diffus. Forum* **2006**, *249*, 255–262. [CrossRef]

71. Xie, H.; Goodenough, J.B.; Li, Y. Li$_{1.2}$Zr$_{1.9}$Ca$_{0.1}$(PO$_4$)$_3$, a Room-Temperature Li-Ion Solid Electrolyte. *J. Power Sources* **2011**, *196*, 7760–7762. [CrossRef]

72. Smith, S.; Thompson, T.; Sakamoto, J.; Allen, J.L.; Baker, D.R.; Wolfenstine, J. Electrical, Mechanical and Chemical Behavior of Li$_{1.2}$Zr$_{1.9}$Sr$_{0.1}$(PO$_4$)$_3$. *Solid State Ionics* **2017**, *300*, 38–45. [CrossRef]

73. Harada, M.; Takeda, H.; Suzuki, S.; Nakano, K.; Tanibata, N.; Nakayama, M.; Karasuyama, M.; Takeuchi, I. Bayesian-Optimization-Guided Experimental Search of NASICON-Type Solid Electrolytes for All-Solid-State Li-Ion Batteries. *J. Mater. Chem. A* **2020**, *8*, 15103–15109. [CrossRef]

74. Kumar, S.; Balaya, P. Improved Ionic Conductivity in NASICON-Type Sr^{2+} Doped LiZr$_2$(PO$_4$)$_3$. *Solid State Ionics* **2016**, *296*, 1–6. [CrossRef]

75. Lai, Y.; Sun, Z.; Jiang, L.; Hao, X.; Jia, M.; Wang, L.; Liu, F. Rapid Sintering of Ceramic Solid Electrolytes LiZr$_2$(PO$_4$)$_3$ and Li$_{1.2}$Ca$_{0.1}$Zr$_{1.9}$(PO$_4$)$_3$ Using a Microwave Sintering Process at Low Temperatures. *Ceram. Int.* **2019**, *45*, 11068–11072. [CrossRef]

76. Zhang, Y.; Liu, H.; Xie, Z.; Qu, W.; Freschi, D.J.; Liu, J. Progress and Perspectives of Lithium Aluminum Germanium Phosphate-Based Solid Electrolytes for Lithium Batteries. *Adv. Funct. Mater.* **2023**, 2300973. [CrossRef]

77. Dias, J.A.; Santagneli, S.H.; Rodrigues, A.C.M.; Bôas, N.V.; Messaddeq, Y. Understanding the Evolution of the Structure and Electrical Properties during Crystallization of Li$_{1.5}$Al$_{0.5}$Ge$_{1.5}$(PO$_4$)$_3$ and Li$_{1.5}$Sc$_{0.17}$Al$_{0.33}$Ge$_{1.5}$(PO$_4$)$_3$ NASICON -Type Glass Ceramics. *J. Phys. Chem. C* **2023**, *127*, 6207–6225. [CrossRef]

78. Waetzig, K.; Rost, A.; Langklotz, U.; Matthey, B.; Schilm, J. An Explanation of the Microcrack Formation in Li$_{1.3}$Al$_{0.3}$Ti$_{1.7}$(PO$_4$)$_3$ Ceramics. *J. Eur. Ceram. Soc.* **2016**, *36*, 1995–2001. [CrossRef]

79. Davis, C.; Nino, J.C. Microwave Processing for Improved Ionic Conductivity in Li$_2$O–Al$_2$O$_3$ –TiO$_2$–P$_2$O$_5$ Glass-Ceramics. *J. Am. Ceram. Soc.* **2015**, *98*, 2422–2427. [CrossRef]

80. Thokchom, J.S.; Kumar, B. The Effects of Crystallization Parameters on the Ionic Conductivity of a Lithium Aluminum Germanium Phosphate Glass–Ceramic. *J. Power Sources* **2010**, *195*, 2870–2876. [CrossRef]

81. Waetzig, K.; Rost, A.; Heubner, C.; Coeler, M.; Nikolowski, K.; Wolter, M.; Schilm, J. Synthesis and Sintering of Li$_{1.3}$Al$_{0.3}$Ti$_{1.7}$(PO$_4$)$_3$ (LATP) Electrolyte for Ceramics with Improved Li+ Conductivity. *J. Alloys Compd.* **2020**, *818*, 153237. [CrossRef]

82. Vizgalov, V.A.; Nestler, T.; Trusov, L.A.; Bobrikov, I.A.; Ivankov, O.I.; Avdeev, M.V.; Motylenko, M.; Brendler, E.; Vyalikh, A.; Meyer, D.C.; et al. Enhancing Lithium-Ion Conductivity in NASICON Glass-Ceramics by Adding Yttria. *CrystEngComm* **2018**, *20*, 1375–1382. [CrossRef]

83. Jadhav, H.S.; Cho, M.-S.; Kalubarme, R.S.; Lee, J.-S.; Jung, K.-N.; Shin, K.-H.; Park, C.-J. Influence of B_2O_3 Addition on the Ionic Conductivity of $Li_{1.5}Al_{0.5}Ge_{1.5}(PO_4)_3$ Glass Ceramics. *J. Power Sources* **2013**, *241*, 502–508. [CrossRef]

84. Liu, Z.; Venkatachalam, S.; Kirchhain, H.; van Wüllen, L. Study of the Glass-to-Crystal Transformation of the NASICON-Type Solid Electrolyte $Li_{1+x}Al_xGe_{2−x}(PO_4)_3$. *Solid State Ionics* **2016**, *295*, 32–40. [CrossRef]

85. Yao, Z.; Zhu, K.; Zhang, J.; Li, X.; Chen, J.; Wang, J.; Yan, K.; Liu, J. Co-Precipitation Synthesis and Electrochemical Properties of NASICON-Type Li1.3Al0.3Ti1.7(PO4)3 Solid Electrolytes. *J. Mater. Sci. Mater. Electron.* **2021**, *32*, 24834–24844. [CrossRef]

86. Delaizir, G.; Viallet, V.; Aboulaich, A.; Bouchet, R.; Tortet, L.; Seznec, V.; Morcrette, M.; Tarascon, J.-M.; Rozier, P.; Dollé, M. The Stone Age Revisited: Building a Monolithic Inorganic Lithium-Ion Battery. *Adv. Funct. Mater.* **2012**, *22*, 2140–2147. [CrossRef]

87. Chang, C.-M.; Lee, Y., II; Hong, S.-H.; Park, H.-M. Spark Plasma Sintering of $LiTi_2(PO_4)_3$-Based Solid Electrolytes. *J. Am. Ceram. Soc.* **2005**, *88*, 1803–1807. [CrossRef]

88. Hallopeau, L.; Bregiroux, D.; Rousse, G.; Portehault, D.; Stevens, P.; Toussaint, G.; Laberty-Robert, C. Microwave-Assisted Reactive Sintering and Lithium Ion Conductivity of $Li_{1.3}Al_{0.3}Ti_{1.7}(PO_4)_3$ Solid Electrolyte. *J. Power Sources* **2018**, *378*, 48–52. [CrossRef]

89. Mahmoud, M.; Cui, Y.; Rohde, M.; Ziebert, C.; Link, G.; Seifert, H. Microwave Crystallization of Lithium Aluminum Germanium Phosphate Solid-State Electrolyte. *Materials* **2016**, *9*, 506. [CrossRef]

90. Sun, Z.; Liu, L.; Lu, Y.; Shi, G.; Li, J.; Ma, L.; Zhao, J.; An, H. Preparation and Ionic Conduction of $Li_{1.5}Al_{0.5}Ge_{1.5}(PO_4)_3$ Solid Electrolyte Using Inorganic Germanium as Precursor. *J. Eur. Ceram. Soc.* **2019**, *39*, 402–408. [CrossRef]

91. Ma, F.; Zhao, E.; Zhu, S.; Yan, W.; Sun, D.; Jin, Y.; Nan, C. Preparation and Evaluation of High Lithium Ion Conductivity $Li_{1.3}Al_{0.3}Ti_{1.7}(PO_4)_3$ Solid Electrolyte Obtained Using a New Solution Method. *Solid State Ionics* **2016**, *295*, 7–12. [CrossRef]

92. Kotobuki, M.; Koishi, M.; Kato, Y. Preparation of $Li_{1.5}Al_{0.5}Ti_{1.5}(PO_4)_3$ Solid Electrolyte via a Co-Precipitation Method. *Ionics* **2013**, *19*, 1945–1948. [CrossRef]

93. Mariappan, C.R.; Yada, C.; Rosciano, F.; Roling, B. Correlation between Micro-Structural Properties and Ionic Conductivity of $Li_{1.5}Al_{0.5}Ge_{1.5}(PO_4)_3$ Ceramics. *J. Power Sources* **2011**, *196*, 6456–6464. [CrossRef]

94. Ji, F.; Xiao, S.; Cheng, J.; Li, D.; Liao, J.; Guo, Y.; Zhang, H.; Zhang, S.; Wei, Y.; Liu, Y.; et al. Low-Cost and Facile Synthesis of LAGP Solid State Electrolyte via a Co-Precipitation Method. *Appl. Phys. Lett.* **2022**, *121*, 023904. [CrossRef]

95. Jiménez, R.; del Campo, A.; Calzada, M.L.; Sanz, J.; Kobylianska, S.D.; Liniova, B.O.; Belous, A.G.; Ragulya, A.V. Improved Conductivity in Tape Casted Li-NASICON Supported Thick Films: Effect of Temperature Treatments and Lamination. *J. Eur. Ceram. Soc.* **2018**, *38*, 1679–1687. [CrossRef]

96. Epp, V.; Ma, Q.; Hammer, E.-M.; Tietz, F.; Wilkening, M. Very Fast Bulk Li Ion Diffusivity in Crystalline $Li_{1.5}Al_{0.5}Ti_{1.5}(PO_4)_3$ as Seen Using NMR Relaxometry. *Phys. Chem. Chem. Phys.* **2015**, *17*, 32115–32121. [CrossRef] [PubMed]

97. Ma, Q.; Xu, Q.; Tsai, C.-L.; Tietz, F.; Guillon, O. A Novel Sol-Gel Method for Large-Scale Production of Nanopowders: Preparation of $Li_{1.5}Al_{0.5}Ti_{1.5}(PO_4)_3$ as an Example. *J. Am. Ceram. Soc.* **2016**, *99*, 410–414. [CrossRef]

98. Zhang, M.; Huang, Z.; Cheng, J.; Yamamoto, O.; Imanishi, N.; Chi, B.; Pu, J.; Li, J. Solid State Lithium Ionic Conducting Thin Film $Li_{1.4}Al_{0.4}Ge_{1.6}(PO_4)_3$ Prepared by Tape Casting. *J. Alloys Compd.* **2014**, *590*, 147–152. [CrossRef]

99. Huang, L.; Wen, Z.; Wu, M.; Wu, X.; Liu, Y.; Wang, X. Electrochemical Properties of $Li_{1.4}Al_{0.4}Ti_{1.6}(PO_4)_3$ Synthesized by a Co-Precipitation Method. *J. Power Sources* **2011**, *196*, 6943–6946. [CrossRef]

100. Duluard, S.; Paillassa, A.; Lenormand, P.; Taberna, P.-L.; Simon, P.; Rozier, P.; Ansart, F. Dense on Porous Solid LATP Electrolyte System: Preparation and Conductivity Measurement. *J. Am. Ceram. Soc.* **2017**, *100*, 141–149. [CrossRef]

101. Chung, H.; Kang, B. Increase in Grain Boundary Ionic Conductivity of $Li_{1.5}Al_{0.5}Ge_{1.5}(PO_4)_3$ by Adding Excess Lithium. *Solid State Ionics* **2014**, *263*, 125–130. [CrossRef]

102. Safanama, D.; Adams, S. High Efficiency Aqueous and Hybrid Lithium-Air Batteries Enabled by $Li_{1.5}Al_{0.5}Ge_{1.5}(PO_4)_3$ Ceramic Anode-Protecting Membranes. *J. Power Sources* **2017**, *340*, 294–301. [CrossRef]

103. Yang, J.; Huang, Z.; Huang, B.; Zhou, J.; Xu, X. Influence of Phosphorus Sources on Lithium Ion Conducting Performance in the System of Li_2O–Al_2O_3–GeO_2–P_2O_5 Glass–Ceramics. *Solid State Ionics* **2015**, *270*, 61–65. [CrossRef]

104. Cui, Y.; Mahmoud, M.M.; Rohde, M.; Ziebert, C.; Seifert, H.J. Thermal and Ionic Conductivity Studies of Lithium Aluminum Germanium Phosphate Solid-State Electrolyte. *Solid State Ionics* **2016**, *289*, 125–132. [CrossRef]

105. Kun, H.; Yanhang, W.; Chengkui, Z.; Huifeng, Z.; Yonghua, L.; Jiang, C.; Bin, H.; Juanrong, M. Influence of Al_2O_3 Additions on Crystallization Mechanism and Conductivity of Li_2O–Ge_2O–P_2O_5 Glass–Ceramics. *Phys. B Condens. Matter* **2011**, *406*, 3947–3950. [CrossRef]

106. Berbano, S.S.; Guo, J.; Guo, H.; Lanagan, M.T.; Randall, C.A. Cold Sintering Process of $Li_{1.5}Al_{0.5}Ge_{1.5}(PO_4)_3$ Solid Electrolyte. *J. Am. Ceram. Soc.* **2017**, *100*, 2123–2135. [CrossRef]

107. Kubanska, A.; Castro, L.; Tortet, L.; Schäf, O.; Dollé, M.; Bouchet, R. Elaboration of Controlled Size $Li_{1.5}Al_{0.5}Ge_{1.5}(PO_4)_3$ Crystallites from Glass-Ceramics. *Solid State Ionics* **2014**, *266*, 44–50. [CrossRef]

108. Fu, J. Fast Li+ Ion Conducting Glass-Ceramics in the System Li_2O–Al_2O_3–GeO_2–P_2O_5. *Solid State Ionics* **1997**, *104*, 191–194. [CrossRef]

109. Cruz, A.M.; Ferreira, E.B.; Rodrigues, A.C.M. Controlled Crystallization and Ionic Conductivity of a Nanostructured $LiAlGePO_4$ Glass–Ceramic. *J. Non-Cryst. Solids* **2009**, *355*, 2295–2301. [CrossRef]

110. Xu, X.; Wen, Z.; Wu, X.; Yang, X.; Gu, Z. Lithium Ion-Conducting Glass-Ceramics of $Li_{1.5}Al_{0.5}Ge_{1.5}(PO_4)_3$ -XLi_2O (X = 0.0–0.20) with Good Electrical and Electrochemical Properties. *J. Am. Ceram. Soc.* **2007**, *90*, 2802–2806. [CrossRef]

111. Borik, M.A.; Bredikhin, S.I.; Bublik, V.T.; Kulebyakin, A.V.; Kuritsyna, I.E.; Lomonova, E.E.; Milovich, P.O.; Myzina, V.A.; Osiko, V.V.; Ryabochkina, P.A.; et al. Structure and Conductivity of Yttria and Scandia-Doped Zirconia Crystals Grown by Skull Melting. *J. Am. Ceram. Soc.* **2017**, *100*, 5536–5547. [CrossRef]

112. Arbi, K.; París, M.A.; Sanz, J. Lithium Exchange Processes in the Conduction Network of the Nasicon $LiTi_{2-x}Zr_x(PO_4)_3$ Series ($0 \leq x \leq 2$). *J. Phys. Chem. B* **2006**, *110*, 6454–6457. [CrossRef]

113. Zhang, P.; Matsui, M.; Hirano, A.; Takeda, Y.; Yamamoto, O.; Imanishi, N. Water-Stable Lithium Ion Conducting Solid Electrolyte of the $Li_{1.4}Al_{0.4}Ti_{1.6-x}Ge_x(PO_4)_3$ System (X = 0–1.0) with NASICON-Type Structure. *Solid State Ionics* **2013**, *253*, 175–180. [CrossRef]

114. Kyono, N.; Bai, F.; Nemori, H.; Minami, H.; Mori, D.; Takeda, Y.; Yamamoto, O.; Imanishi, N. Lithium-Ion Conducting Solid Electrolytes of $Li_{1.4}Al_{0.4}Ge_{0.2}Ti_{1.4}(PO_4)_3$ and MO_x (M = Al, Ti, and Zr) Composites. *Solid State Ionics* **2018**, *324*, 114–127. [CrossRef]

115. Saffirio, S.; Falco, M.; Appetecchi, G.B.; Smeacetto, F.; Gerbaldi, C. $Li_{1.4}Al_{0.4}Ge_{0.4}Ti_{1.4}(PO_4)_3$ Promising NASICON-Structured Glass-Ceramic Electrolyte for All-Solid-State Li-Based Batteries: Unravelling the Effect of Diboron Trioxide. *J. Eur. Ceram. Soc.* **2022**, *42*, 1023–1032. [CrossRef]

116. Salkus, T.; Dindune, A.; Kanepe, Z.; Ronis, J.; Urcinskas, A.; Kezionis, A.; Orliukas, A. Lithium Ion Conductors in the System $Li_{1+y}Ge_{2-x-y}Ti_xAl_y(PO_4)_3$ (X=0.1÷0.3, Y=0.07÷0.21). *Solid State Ionics* **2007**, *178*, 1282–1287. [CrossRef]

117. Maldonado-Manso, P.; Losilla, E.R.; Martínez-Lara, M.; Aranda, M.A.G.; Bruque, S.; Mouahid, F.E.; Zahir, M. High Lithium Ionic Conductivity in the $Li_{1+x}Al_xGe_yTi_{2-x-y}(PO_4)_3$ NASICON Series. *Chem. Mater.* **2003**, *15*, 1879–1885. [CrossRef]

118. Hartmann, P.; Leichtweiss, T.; Busche, M.R.; Schneider, M.; Reich, M.; Sann, J.; Adelhelm, P.; Janek, J. Degradation of NASICON-Type Materials in Contact with Lithium Metal: Formation of Mixed Conducting Interphases (MCI) on Solid Electrolytes. *J. Phys. Chem. C* **2013**, *117*, 21064–21074. [CrossRef]

119. Nuernberg, R.B.; Basbus, J.F.; Lux, K.C.; Sainz, M.P.; Cuello, G.J.; Rodrigues, A.C.M.; Piarristeguy, A.A.; Ribes, M.; Pradel, A. Correlation between Structural Features and Ionic Transport in Lithium-Ion Conducting Glass–Ceramics from the $Li_{1+x}Cr_xGeTi_{1-x}(PO_4)_3$ System. *J. Phys. Chem. C* **2022**, *126*, 4584–4592. [CrossRef]

120. Xu, A.; Wang, R.; Yao, M.; Cao, J.; Li, M.; Yang, C.; Liu, F.; Ma, J. Electrochemical Properties of an Sn-Doped LATP Ceramic Electrolyte and Its Derived Sandwich-Structured Composite Solid Electrolyte. *Nanomaterials* **2022**, *12*, 2082. [CrossRef]

121. Stenina, I.; Pyrkova, A.; Yaroslavtsev, A. NASICON-Type $Li_{1+x}Al_xZr_yTi_{2-x-y}(PO_4)_3$ Solid Electrolytes: Effect of Al, Zr Co-Doping and Synthesis Method. *Batteries* **2023**, *9*, 59. [CrossRef]

122. Rai, K.; Kundu, S. Fabrication and Performances of High Lithium-Ion Conducting Solid Electrolytes Based on NASICON $Li_{1.3}Al_{0.3}Ti_{1.7-X}Zr_x(PO_4)_3$ ($0 \leq X \leq 0.2$). *Ceram. Int.* **2020**, *46*, 23695–23705. [CrossRef]

123. Kothari, D.H.; Kanchan, D.K. Effect of Doping of Trivalent Cations Ga^{3+}, Sc^{3+}, Y^{3+} in $Li_{1.3}Al_{0.3}Ti_{1.7}(PO_4)_3$ (LATP) System on Li + Ion Conductivity. *Phys. B Condens. Matter* **2016**, *501*, 90–94. [CrossRef]

124. Zhang, P.; Matsui, M.; Takeda, Y.; Yamamoto, O.; Imanishi, N. Water-Stable Lithium Ion Conducting Solid Electrolyte of Iron and Aluminum Doped NASICON-Type $LiTi_2(PO_4)_3$. *Solid State Ionics* **2014**, *263*, 27–32. [CrossRef]

125. Wang, S.-F.; Shieh, D.; Ko, Y.-A.; Hsu, Y.-F.; Wu, M.-K. Structural and Electrical Studies of B^{3+}-and-In^{3+}-Ion Co-Doped $Li_{1.3}Al_{0.3}Ti_{1.7}(PO_4)_3$ Solid Electrolytes. *Solid State Ionics* **2023**, *393*, 116174. [CrossRef]

126. Ioanniti, M.M.; Tenhaeff, W.E. Enhancing the Stability of Lithium Ion $Li_{1+x+y}Al_xTi_{2-x}Si_yP_{3-y}O_{12}$ Glass—Ceramic Conductors in Aqueous Electrolytes. *J. Power Sources* **2017**, *371*, 209–216. [CrossRef]

127. Kundu, S.; Ein-Eli, Y. A Review on Design Considerations in Polymer and Polymer Composite Solid-State Electrolytes for Solid Li Batteries. *J. Power Sources* **2023**, *553*, 232267. [CrossRef]

128. Mashekova, A.; Baltash, Y.; Yegamkulov, M.; Trussov, I.; Bakenov, Z.; Mukanova, A. Polycationic Doping of the LATP Ceramic Electrolyte for Li-Ion Batteries. *RSC Adv.* **2022**, *12*, 29595–29601. [CrossRef]

129. Cui, C.; Zeng, C.; Huang, G.; Feng, X.; Zhang, Y.; Zhai, T.; Li, H. In Situ Visualizing the Interfacial Failure Mechanism and Modification Promotion of LAGP Solid Electrolyte toward Li Metal Anode. *Adv. Energy Mater.* **2022**, *12*, 2202250. [CrossRef]

130. Han, F.; Westover, A.S.; Yue, J.; Fan, X.; Wang, F.; Chi, M.; Leonard, D.N.; Dudney, N.J.; Wang, H.; Wang, C. High Electronic Conductivity as the Origin of Lithium Dendrite Formation within Solid Electrolytes. *Nat. Energy* **2019**, *4*, 187–196. [CrossRef]

131. Zhao, Q.; Stalin, S.; Zhao, C.-Z.; Archer, L.A. Designing Solid-State Electrolytes for Safe, Energy-Dense Batteries. *Nat. Rev. Mater.* **2020**, *5*, 229–252. [CrossRef]

132. Aizat Razali, A.; Norazli, S.N.; Sum, W.S.; Yeo, S.Y.; Dolfi, A.; Srinivasan, G. State-of-the-Art of Solid-State Electrolytes on the Road Map of Solid-State Lithium Metal Batteries for E-Mobility. *ACS Sustain. Chem. Eng.* **2023**, *11*, 7927–7964. [CrossRef]

133. Tolganbek, N.; Serikkazyyeva, A.; Kalybekkyzy, S.; Sarsembina, M.; Kanamura, K.; Bakenov, Z.; Mentbayeva, A. Interface Modification of NASICON-Type Li-Ion Conducting Ceramic Electrolytes: A Critical Evaluation. *Mater. Adv.* **2022**, *3*, 3055–3069. [CrossRef]

134. Li, S.; Chen, Z.; Zhang, W.; Li, S.; Pan, F. High-Throughput Screening of Protective Layers to Stabilize the Electrolyte-Anode Interface in Solid-State Li-Metal Batteries. *Nano Energy* **2022**, *102*, 107640. [CrossRef]

135. Hao, X.; Zhao, Q.; Su, S.; Zhang, S.; Ma, J.; Shen, L.; Yu, Q.; Zhao, L.; Liu, Y.; Kang, F.; et al. Constructing Multifunctional Interphase between $Li_{1.4}Al_{0.4}Ti_{1.6}(PO_4)_3$ and Li Metal by Magnetron Sputtering for Highly Stable Solid-State Lithium Metal Batteries. *Adv. Energy Mater.* **2019**, *9*, 1901604. [CrossRef]

136. Lei, M.; Fan, S.; Yu, Y.; Hu, J.; Chen, K.; Gu, Y.; Wu, C.; Zhang, Y.; Li, C. NASICON-Based Solid State Li-Fe-F Conversion Batteries Enabled by Multi-Interface-Compatible Sericin Protein Buffer Layer. *Energy Storage Mater.* **2022**, *47*, 551–560. [CrossRef]

137. Liu, F.; Chuan, X.; Yang, Y.; Huang, D.; He, X. Stable Cycling of Solid-State Lithium Metal Batteries at Room Temperature via Reducing Electrode/Electrolyte Interfacial Resistance. *J. Mater. Eng. Perform.* **2021**, *30*, 4543–4551. [CrossRef]

138. Chen, Z.; Kim, G.; Kim, J.; Zarrabeitia, M.; Kuenzel, M.; Liang, H.; Geiger, D.; Kaiser, U.; Passerini, S. Highly Stable Quasi-Solid-State Lithium Metal Batteries: Reinforced $Li_{1.3}Al_{0.3}Ti_{1.7}(PO_4)_3$/Li Interface by a Protection Interlayer. *Adv. Energy Mater.* **2021**, *11*, 2101339. [CrossRef]

139. Pan, L.; Sun, S.; Yu, G.; Liu, X.X.; Feng, S.; Zhang, W.; Turgunov, M.; Wang, Y.; Sun, Z. Stabilizing Solid Electrolyte/Li Interface via Polymer-in-Salt Artificial Protection Layer for High-Rate and Stable Lithium Metal Batteries. *Chem. Eng. J.* **2022**, *449*, 137682. [CrossRef]

140. Bai, H.; Hu, J.; Duan, Y.; Kozawa, T.; Naito, M.; Zhang, J.; Dong, S. Surface Modification of $Li_{1.3}Al_{0.3}Ti_{1.7}(PO_4)_3$ Ceramic Electrolyte by Al_2O_3-Doped ZnO Coating to Enable Dendrites-Free All-Solid-State Lithium-Metal Batteries. *Ceram. Int.* **2019**, *45*, 14663–14668. [CrossRef]

141. Li, C.-F.; Muruganantham, R.; Hsu, W.-C.; Ihrig, M.; Hsieh, C.-T.; Wang, C.-C.; Liu, W.-R. Atomic Layer Deposition of ZnO on $Li_{1.3}Al_{0.3}Ti_{1.7}(PO_4)_3$ Enables Its Application in All Solid-State Lithium Batteries. *J. Taiwan Inst. Chem. Eng.* **2023**, *144*, 104681. [CrossRef]

142. Ci, N.; Zhang, L.; Li, J.; Li, D.; Cheng, J.; Sun, Q.; Xi, Z.; Xu, Z.; Zhao, G.; Ci, L. In Situ Construction of a Flexible Interlayer for Durable Solid-State Lithium Metal Batteries. *Carbon* **2022**, *187*, 13–21. [CrossRef]

143. Liu, Y.; Sun, Q.; Zhao, Y.; Wang, B.; Kaghazchi, P.; Adair, K.R.; Li, R.; Zhang, C.; Liu, J.; Kuo, L.-Y.; et al. Stabilizing the Interface of NASICON Solid Electrolyte against Li Metal with Atomic Layer Deposition. *ACS Appl. Mater. Interfaces* **2018**, *10*, 31240–31248. [CrossRef] [PubMed]

144. Sun, Z.; Liu, L.; Yang, B.; Li, Q.; Wu, B.; Zhao, J.; Ma, L.; Liu, Y.; An, H. Preparation and Ion Conduction of $Li_{1.5}Al_{0.5}Ge_{1.5}(PO_4)_3$ Solid Electrolyte Films Using Radio Frequency Sputtering. *Solid State Ionics* **2020**, *346*, 115224. [CrossRef]

145. Cheng, Q.; Li, A.; Li, N.; Li, S.; Zangiabadi, A.; Li, T.-D.; Huang, W.; Li, A.C.; Jin, T.; Song, Q.; et al. Stabilizing Solid Electrolyte-Anode Interface in Li-Metal Batteries by Boron Nitride-Based Nanocomposite Coating. *Joule* **2019**, *3*, 1510–1522. [CrossRef]

146. Liu, L.; Cui, X.; Jie, Z.; Lin, Y.; Zhang, C.; Song, J.; Wang, L.; Ma, J.; Ma, L. Improved Ion Conductivity and Interface Characteristics of the Te-Doped Solid NASICON Electrolyte $Li_{1.5}Al_{0.5}Ge_{1.5}(PO_4)_3$ with Graphite Coating. *J. Power Sources* **2023**, *575*, 233137. [CrossRef]

147. Liu, L.; Wang, Q.; Jie, Z.; Ma, J.; Cui, X.; Xu, G.; Gu, C.; Ma, L.; Liu, Y. Stable Interface between Anode Materials and $Li_{1.3}Al_{0.3}Ti_{1.7}(PO_4)_3$-Based Solid-State Electrolyte Facilitated by Graphene Coating. *Electrochim. Acta* **2022**, *431*, 141136. [CrossRef]

148. Hao, X.; Chen, K.; Tang, Y.; Zhong, X.; Cai, K. 2-Dimensional g-C3N4 Nanosheets Modified LATP-Based "Polymer-in-Ceramic" Electrolyte for Solid-State Lithium Batteries. *J. Alloys Compd.* **2023**, *942*, 169064. [CrossRef]

149. Lee, S.; Jung, S.; Yang, S.; Lee, J.-H.; Shin, H.; Kim, J.; Park, S. Revisiting the LiPON/Li Thin Film as a Bifunctional Interlayer for NASICON Solid Electrolyte-Based Lithium Metal Batteries. *Appl. Surf. Sci.* **2022**, *586*, 152790. [CrossRef]

150. Yu, J.; Liu, Q.; Hu, X.; Wang, S.; Wu, J.; Liang, B.; Han, C.; Kang, F.; Li, B. Smart Construction of Multifunctional $Li_{1.5}Al_{0.5}Ge_{1.5}(PO_4)_3$ | Li Intermediate Interfaces for Solid-State Batteries. *Energy Storage Mater.* **2022**, *46*, 68–75. [CrossRef]

151. Zha, W.; Ruan, Y.; Wen, Z. A Janus $Li_{1.5}Al_{0.5}Ge_{1.5}(PO_4)_3$ with High Critical Current Density for High-Voltage Lithium Batteries. *Chem. Eng. J.* **2022**, *429*, 132506. [CrossRef]

152. Tang, J.; Wang, L.; Tian, C.; Chen, C.; Huang, T.; Zeng, L.; Yu, A. Double-Protected Layers with Solid–Liquid Hybrid Electrolytes for Long-Cycle-Life Lithium Batteries. *ACS Appl. Mater. Interfaces* **2022**, *14*, 4170–4178. [CrossRef]

153. Tang, J.; Wang, L.; Tian, C.; Huang, T.; Zeng, L.; Yu, A. Comparative Performance of LiFePO4 and $LiNi_{0.6}Co_{0.2}Mn_{0.2}O_2$ Cathode Materials for Lithium Batteries with Solid–Liquid Hybrid Electrolytes. *J. Power Sources* **2021**, *515*, 230639. [CrossRef]

154. Sun, S.; Zhao, C.-Z.; Yuan, H.; Lu, Y.; Hu, J.-K.; Huang, J.-Q.; Zhang, Q. Multiscale Understanding of High-Energy Cathodes in Solid-State Batteries: From Atomic Scale to Macroscopic Scale. *Mater. Futures* **2022**, *1*, 012101. [CrossRef]

155. Paolella, A.; Zhu, W.; Campanella, D.; Kaboli, S.; Feng, Z.; Vijh, A. NASICON Lithium Ions Conductors: Materials, Composites, and Batteries. *Curr. Opin. Electrochem.* **2022**, *36*, 101108. [CrossRef]

156. Zheng, F.; Song, Z.; Li, H.; Zheng, Y.-Z.; Tao, X. Distinct Functional Janus Interfaces for Dendrite-Free $Li_{1.3}Al_{0.3}Ti_{1.7}(PO_4)_3$-Based Lithium Metal Batteries. *Electrochim. Acta* **2022**, *436*, 141395. [CrossRef]

157. Overhoff, G.M.; Ali, M.Y.; Brinkmann, J.-P.; Lennartz, P.; Orthner, H.; Hammad, M.; Wiggers, H.; Winter, M.; Brunklaus, G. Ceramic-in-Polymer Hybrid Electrolytes with Enhanced Electrochemical Performance. *ACS Appl. Mater. Interfaces* **2022**, *14*, 53636–53647. [CrossRef] [PubMed]

158. Yu, S.; Xu, Q.; Lu, X.; Liu, Z.; Windmüller, A.; Tsai, C.-L.; Buchheit, A.; Tempel, H.; Kungl, H.; Wiemhöfer, H.-D.; et al. Single-Ion-Conducting "Polymer-in-Ceramic" Hybrid Electrolyte with an Intertwined NASICON-Type Nanofiber Skeleton. *ACS Appl. Mater. Interfaces* **2021**, *13*, 61067–61077. [CrossRef] [PubMed]

159. Shi, X.; Ma, N.; Wu, Y.; Lu, Y.; Xiao, Q.; Li, Z.; Lei, G. Fabrication and Electrochemical Properties of LATP/PVDF Composite Electrolytes for Rechargeable Lithium-Ion Battery. *Solid State Ionics* **2018**, *325*, 112–119. [CrossRef]

160. Zhang, K.; Mu, S.; Liu, W.; Zhu, D.; Ding, Z.; Chen, Y. A Flexible NASICON-Type Composite Electrolyte for Lithium-Oxygen/Air Battery. *Ionics* **2019**, *25*, 25–33. [CrossRef]

161. Panneerselvam, T.; Rajamani, A.; Janani, N.; Murugan, R.; Sivaprakasam, S. Electrospun Composite Polymer Electrolyte for High-Performance Quasi Solid-State Lithium Metal Batteries. *Ionics* **2023**, *29*, 1395–1406. [CrossRef]

162. Wang, C.; Sun, Q.; Liu, Y.; Zhao, Y.; Li, X.; Lin, X.; Banis, M.N.; Li, M.; Li, W.; Adair, K.R.; et al. Boosting the Performance of Lithium Batteries with Solid-Liquid Hybrid Electrolytes: Interfacial Properties and Effects of Liquid Electrolytes. *Nano Energy* **2018**, *48*, 35–43. [CrossRef]

163. Tang, J.; Wang, L.; You, L.; Chen, X.; Huang, T.; Zhou, L.; Geng, Z.; Yu, A. Effect of Organic Electrolyte on the Performance of Solid Electrolyte for Solid–Liquid Hybrid Lithium Batteries. *ACS Appl. Mater. Interfaces* **2021**, *13*, 2685–2693. [CrossRef] [PubMed]

164. Martínez-Cisneros, C.S.; Pandit, B.; Antonelli, C.; Sanchez, J.Y.; Levenfeld, B.; Varez, A. Development of Sodium Hybrid Quasi-Solid Electrolytes Based on Porous NASICON and Ionic Liquids. *J. Eur. Ceram. Soc.* **2021**, *41*, 7723–7733. [CrossRef]

165. Lei, W.; Zhang, C.; Qiao, R.; Ravivarma, M.; Chen, H.; Ajdari, F.B.; Salavati-Niasari, M.; Song, J. Stable Li | LAGP Interface Enabled by Confining Solvate Ionic Liquid in a Hyperbranched Polyanionic Copolymer for NASICON-Based Solid-State Batteries. *ACS Appl. Energy Mater.* **2023**, *6*, 4363–4371. [CrossRef]

166. Il'ina, E.; Druzhinin, K.; Lyalin, E.; Talankin, I. In Situ Li-In Anode Formation on the $Li_7La_3Zr_2O_{12}$ Solid Electrolyte in All-Solid-State Battery. *Batteries* **2022**, *8*, 226. [CrossRef]

167. He, M.; Cui, Z.; Chen, C.; Li, Y.; Guo, X. Formation of Self-Limited, Stable and Conductive Interfaces between Garnet Electrolytes and Lithium Anodes for Reversible Lithium Cycling in Solid-State Batteries. *J. Mater. Chem. A* **2018**, *6*, 11463–11470. [CrossRef]

168. Tsai, C.-L.; Roddatis, V.; Chandran, C.V.; Ma, Q.; Uhlenbruck, S.; Bram, M.; Heitjans, P.; Guillon, O. $Li_7La_3Zr_2O_{12}$ Interface Modification for Li Dendrite Prevention. *ACS Appl. Mater. Interfaces* **2016**, *8*, 10617–10626. [CrossRef]

169. El-Shinawi, H.; Regoutz, A.; Payne, D.J.; Cussen, E.J.; Corr, S.A. NASICON $LiM_2(PO_4)_3$ Electrolyte (M = Zr) and Electrode (M = Ti) Materials for All Solid-State Li-Ion Batteries with High Total Conductivity and Low Interfacial Resistance. *J. Mater. Chem. A* **2018**, *6*, 5296–5303. [CrossRef]

170. Kee, Y.; Dimov, N.; Kobayashi, E.; Kitajou, A.; Okada, S. Structural and Electrochemical Properties of Fe- and Al-Doped $Li_3V_2(PO_4)_3$ for All-Solid-State Symmetric Lithium Ion Batteries Prepared by Spray-Drying-Assisted Carbothermal Method. *Solid State Ionics* **2015**, *272*, 138–143. [CrossRef]

171. Bates, A.M.; Preger, Y.; Torres-Castro, L.; Harrison, K.L.; Harris, S.J.; Hewson, J. Are Solid-State Batteries Safer than Lithium-Ion Batteries? *Joule* **2022**, *6*, 742–755. [CrossRef]

172. Liang, J.; Zhang, X.; Zeng, X.; Yan, M.; Yin, Y.; Xin, S.; Wang, W.; Wu, X.; Shi, J.; Wan, L.; et al. Enabling a Durable Electrochemical Interface via an Artificial Amorphous Cathode Electrolyte Interphase for Hybrid Solid/Liquid Lithium-Metal Batteries. *Angew. Chem.* **2020**, *132*, 6647–6651. [CrossRef]

173. Wu, D.; Wu, F. Toward Better Batteries: Solid-State Battery Roadmap 2035+. *eTransportation* **2023**, *16*, 100224. [CrossRef]

174. Schmaltz, T.; Wicke, T.; Weymann, L.; Voß, P.; Neef, C.; Thielmann, A. *Solid-State Battery Roadmap 2035+*; Fraunhofer ISI: Karlsruhe, Germany, 2022; 112p.

175. Alloina, F.; Iojoiu, C. 4—Composite Polymer Electrolytes for Electrochemical Devices. In *Polymer Electrolytes*; Sequeira, C., Santos, D., Eds.; Woodhead Publishing: Shaxton, UK, 2010; pp. 129–175. ISBN 978-1-84569-772-3.

176. Liang, C.C. Conduction Characteristics of the Lithium Iodide-Aluminum Oxide Solid Electrolytes. *J. Electrochem. Soc.* **1973**, *120*, 1289. [CrossRef]

177. Maier, J. Ionic Conduction in Space Charge Regions. *Prog. Solid State Chem.* **1995**, *23*, 171–263. [CrossRef]

178. Voropaeva, D.Y.; Novikova, S.A.; Yaroslavtsev, A.B. Polymer Electrolytes for Metal-Ion Batteries. *Russ. Chem. Rev.* **2020**, *89*, 1132–1155. [CrossRef]

179. Zhang, Z.; Wang, X.; Li, X.; Zhao, J.; Liu, G.; Yu, W.; Dong, X.; Wang, J. Review on Composite Solid Electrolytes for Solid-State Lithium-Ion Batteries. *Mater. Today Sustain.* **2023**, *21*, 100316. [CrossRef]

180. Li, D.; Qin, D.; Nie, F.; Wen, L.; Xue, L. Enhancement of Electrochemical Performance of Lithium-Ion Battery by Single-Ion Conducting Polymer Addition in Ceramic-Coated Separator. *J. Mater. Sci.* **2018**, *53*, 11038–11049. [CrossRef]

181. Hanemann, T.; Szabó, D.V. Polymer-Nanoparticle Composites: From Synthesis to Modern Applications. *Materials* **2010**, *3*, 3468–3517. [CrossRef]

182. Koizumi, Y.; Mori, D.; Taminato, S.; Yamamoto, O.; Takeda, Y.; Imanishi, N. Lithium-Stable NASICON-Type Lithium-Ion Conducting Solid Electrolyte Film Coated with a Polymer Electrolyte. *Solid State Ionics* **2019**, *337*, 101–106. [CrossRef]

183. Bonizzoni, S.; Ferrara, C.; Berbenni, V.; Anselmi-Tamburini, U.; Mustarelli, P.; Tealdi, C. NASICON-Type Polymer-in-Ceramic Composite Electrolytes for Lithium Batteries. *Phys. Chem. Chem. Phys.* **2019**, *21*, 6142–6149. [CrossRef]

184. Zhai, H.; Xu, P.; Ning, M.; Cheng, Q.; Mandal, J.; Yang, Y. A Flexible Solid Composite Electrolyte with Vertically Aligned and Connected Ion-Conducting Nanoparticles for Lithium Batteries. *Nano Lett.* **2017**, *17*, 3182–3187. [CrossRef]

185. Han, S.; Liu, S.; Gao, J.; Zhai, M.; Wu, Y.; Tong, J.; Zhang, H.; Tang, W. A Novel Composite Polymer Electrolyte Containing the Lithium-Ion Conductor $Li_3Zr_2Si_2PO_{12}$ Synthesized by Cationic-Exchange Method for Solid Lithium Metal Batteries. *Electrochim. Acta* **2023**, *441*, 141795. [CrossRef]

186. Freitag, A.; Langklotz, U.; Rost, A.; Stamm, M.; Ionov, L. Ionically Conductive Polymer/Ceramic Separator for Lithium-Sulfur Batteries. *Energy Storage Mater.* **2017**, *9*, 105–111. [CrossRef]

187. Maurya, D.K.; Dhanusuraman, R.; Guo, Z.; Angaiah, S. Composite Polymer Electrolytes: Progress, Challenges, and Future Outlook for Sodium-Ion Batteries. *Adv. Compos. Hybrid Mater.* **2022**, *5*, 2651–2674. [CrossRef]

188. Deiner, L.J.; Gothard, N.W.; Buckley, J.; Clarkson, D.; Greenbaum, S.; Rubin, I.; Noga, M.; McGinn, C.; Hsieh, E.; Kymissis, I.; et al. Mechanochemical Synthesis of LAGP/PEG Hybrid Solid Electrolyte: Investigation of Surface Structure and Chemistry. *Solid State Ionics* **2023**, *394*, 116191. [CrossRef]

189. Cheng, J.; Hou, G.; Sun, Q.; Liang, Z.; Xu, X.; Guo, J.; Dai, L.; Li, D.; Nie, X.; Zeng, Z.; et al. Cold-Pressing PEO/LAGP Composite Electrolyte for Integrated All-Solid-State Lithium Metal Battery. *Solid State Ionics* **2020**, *345*, 115156. [CrossRef]

190. Li, Y.; Wang, F.; Huang, B.; Huang, C.; Pei, D.; Liu, Z.; Yuan, S.; Hou, S.; Cao, G.; Jin, H. A High Power Density Solid Electrolyte Based on Polycaprolactone for High-Performance All-Solid-State Flexible Lithium Batteries. *Electrochim. Acta* **2022**, *424*, 140624. [CrossRef]

191. Zhou, D.; Shanmukaraj, D.; Tkacheva, A.; Armand, M.; Wang, G. Polymer Electrolytes for Lithium-Based Batteries: Advances and Prospects. *Chem* **2019**, *5*, 2326–2352. [CrossRef]

192. Jadhao, S.R.; Joat, R.V. The Effect of Nanofiller on Electrical Conductivity of PVA Based Solid Polymer Electrolyte. *Mater. Today Proc.* **2019**, *15*, 581–585. [CrossRef]

193. Yao, P.; Yu, H.; Ding, Z.; Liu, Y.; Lu, J.; Lavorgna, M.; Wu, J.; Liu, X. Review on Polymer-Based Composite Electrolytes for Lithium Batteries. *Front. Chem.* **2019**, *7*, 522. [CrossRef]

194. Yusuf, S.N.F.; Yusof, S.Z.; Kufian, M.Z.; Teo, L.P. Preparation and Electrical Characterization of Polymer Electrolytes: A Review. *Mater. Today Proc.* **2019**, *17*, 446–458. [CrossRef]

195. Mauger, A.; Julien, C.M.; Paolella, A.; Armand, M.; Zaghib, K. Building Better Batteries in the Solid State: A Review. *Materials* **2019**, *12*, 3892. [CrossRef] [PubMed]

196. Zhu, P.; Zhu, J.; Zang, J.; Chen, C.; Lu, Y.; Jiang, M.; Yan, C.; Dirican, M.; Kalai Selvan, R.; Zhang, X. A Novel Bi-Functional Double-Layer RGO–PVDF/PVDF Composite Nanofiber Membrane Separator with Enhanced Thermal Stability and Effective Polysulfide Inhibition for High-Performance Lithium–Sulfur Batteries. *J. Mater. Chem. A* **2017**, *5*, 15096–15104. [CrossRef]

197. Tang, C.; Hackenberg, K.; Fu, Q.; Ajayan, P.M.; Ardebili, H. High Ion Conducting Polymer Nanocomposite Electrolytes Using Hybrid Nanofillers. *Nano Lett.* **2012**, *12*, 1152–1156. [CrossRef] [PubMed]

198. Varzi, A.; Thanner, K.; Scipioni, R.; Di Lecce, D.; Hassoun, J.; Dörfler, S.; Altheus, H.; Kaskel, S.; Prehal, C.; Freunberger, S.A. Current Status and Future Perspectives of Lithium Metal Batteries. *J. Power Sources* **2020**, *480*, 228803. [CrossRef]

199. Zheng, J.; Hu, Y.-Y. New Insights into the Compositional Dependence of Li-Ion Transport in Polymer–Ceramic Composite Electrolytes. *ACS Appl. Mater. Interfaces* **2018**, *10*, 4113–4120. [CrossRef]

200. Yang, T.; Zheng, J.; Cheng, Q.; Hu, Y.-Y.; Chan, C.K. Composite Polymer Electrolytes with $Li_7La_3Zr_2O_{12}$ Garnet-Type Nanowires as Ceramic Fillers: Mechanism of Conductivity Enhancement and Role of Doping and Morphology. *ACS Appl. Mater. Interfaces* **2017**, *9*, 21773–21780. [CrossRef]

201. Zhao, C.-Z.; Zhang, X.-Q.; Cheng, X.-B.; Zhang, R.; Xu, R.; Chen, P.-Y.; Peng, H.-J.; Huang, J.-Q.; Zhang, Q. An Anion-Immobilized Composite Electrolyte for Dendrite-Free Lithium Metal Anodes. *Proc. Natl. Acad. Sci. USA* **2017**, *114*, 11069–11074. [CrossRef]

202. Zheng, J.; Tang, M.; Hu, Y. Lithium Ion Pathway within $Li_7La_3Zr_2O_{12}$-Polyethylene Oxide Composite Electrolytes. *Angew. Chem.* **2016**, *128*, 12726–12730. [CrossRef]

203. Popovic, J.; Brandell, D.; Ohno, S.; Hatzell, K.B.; Zheng, J.; Hu, Y.-Y. Polymer-Based Hybrid Battery Electrolytes: Theoretical Insights, Recent Advances and Challenges. *J. Mater. Chem. A* **2021**, *9*, 6050–6069. [CrossRef]

204. Li, M.; Kolek, M.; Frerichs, J.E.; Sun, W.; Hou, X.; Hansen, M.R.; Winter, M.; Bieker, P. Investigation of Polymer/Ceramic Composite Solid Electrolyte System: The Case of PEO/LGPS Composite Electrolytes. *ACS Sustain. Chem. Eng.* **2021**, *9*, 11314–11322. [CrossRef]

205. Bain, A.D. Chemical Exchange in NMR. *Prog. Nucl. Magn. Reson. Spectrosc.* **2003**, *43*, 63–103. [CrossRef]

206. Zheng, J.; Wang, P.; Liu, H.; Hu, Y.-Y. Interface-Enabled Ion Conduction in $Li_{10}GeP_2S_{12}$ –Poly(Ethylene Oxide) Hybrid Electrolytes. *ACS Appl. Energy Mater.* **2019**, *2*, 1452–1459. [CrossRef]

207. Fu, J.; Li, Z.; Zhou, X.; Guo, X. Ion Transport in Composite Polymer Electrolytes. *Mater. Adv.* **2022**, *3*, 3809–3819. [CrossRef]

208. Yan, Y.; Ju, J.; Dong, S.; Wang, Y.; Huang, L.; Cui, L.; Jiang, F.; Wang, Q.; Zhang, Y.; Cui, G. In Situ Polymerization Permeated Three-Dimensional Li^+ -Percolated Porous Oxide Ceramic Framework Boosting All Solid-State Lithium Metal Battery. *Adv. Sci.* **2021**, *8*, 2003887. [CrossRef] [PubMed]

209. He, L.; Liang, W.-H.; Cao, J.-H.; Wu, D.-Y. PI-LATP-PEO Electrolyte with High Safety Performance in Solid-State Lithium Metal Batteries. *ACS Appl. Energy Mater.* **2022**, *5*, 5277–5286. [CrossRef]

210. Patil, B.H.; Howell, B.R.; Gallaway, J.W. A Multiscale Hollow Spherical LATP Active Filler Improves Conductivity and Mechanical Strength in Composite Solid Electrolytes for Li Batteries. *J. Phys. Chem. C* **2022**, *126*, 15104–15117. [CrossRef]

211. Wang, C.; Huang, D.; Li, S.; Yu, J.; Zhu, M.; Liu, N.; Lu, Z. Three-Dimensional-Percolated Ceramic Nanoparticles along Natural-Cellulose-Derived Hierarchical Networks for High Li + Conductivity and Mechanical Strength. *Nano Lett.* **2020**, *20*, 7397–7404. [CrossRef]

212. Lee, J.; Howell, T.; Rottmayer, M.; Boeckl, J.; Huang, H. Free-Standing PEO/LiTFSI/LAGP Composite Electrolyte Membranes for Applications to Flexible Solid-State Lithium-Based Batteries. *J. Electrochem. Soc.* **2019**, *166*, A416–A422. [CrossRef]

213. Ahmed, S.A.; Pareek, T.; Dwivedi, S.; Badole, M.; Kumar, S. $LiSn_2(PO_4)_3$-Based Polymer-in-Ceramic Composite Electrolyte with High Ionic Conductivity for All-Solid-State Lithium Batteries. *J. Solid State Electrochem.* **2020**, *24*, 2407–2417. [CrossRef]

214. Chen, L.; Li, Y.; Li, S.-P.; Fan, L.-Z.; Nan, C.-W.; Goodenough, J.B. PEO/Garnet Composite Electrolytes for Solid-State Lithium Batteries: From "Ceramic-in-Polymer" to "Polymer-in-Ceramic". *Nano Energy* **2018**, *46*, 176–184. [CrossRef]

215. Bushkova, O.V.; Sanginov, E.A.; Chernyuk, S.D.; Kayumov, R.R.; Shmygleva, L.V.; Dobrovolsky, Y.A.; Yaroslavtsev, A.B. Polymer Electrolytes Based on the Lithium Form of Nafion Sulfonic Cation-Exchange Membranes: Current State of Research and Prospects for Use in Electrochemical Power Sources. *Membr. Membr. Technol.* **2022**, *4*, 433–454. [CrossRef]

216. Deng, K.; Zeng, Q.; Wang, D.; Liu, Z.; Qiu, Z.; Zhang, Y.; Xiao, M.; Meng, Y. Single-Ion Conducting Gel Polymer Electrolytes: Design, Preparation and Application. *J. Mater. Chem. A* **2020**, *8*, 1557–1577. [CrossRef]

217. Zhu, J.; Zhang, Z.; Zhao, S.; Westover, A.S.; Belharouak, I.; Cao, P. Single-Ion Conducting Polymer Electrolytes for Solid-State Lithium–Metal Batteries: Design, Performance, and Challenges. *Adv. Energy Mater.* **2021**, *11*, 2003836. [CrossRef]

218. Voropaeva, D.; Golubenko, D.; Merkel, A.; Yaroslavtsev, A. Membranes with Novel Highly-Delocalized Sulfonylimide Anions for Lithium-Ion Batteries. *J. Membr. Sci.* **2020**, *601*, 117918. [CrossRef]

219. Liu, J.; Pickett, P.D.; Park, B.; Upadhyay, S.P.; Orski, S.V.; Schaefer, J.L. Non-Solvating, Side-Chain Polymer Electrolytes as Lithium Single-Ion Conductors: Synthesis and Ion Transport Characterization. *Polym. Chem.* **2020**, *11*, 461–471. [CrossRef]

220. Ahmed, F.; Choi, I.; Rahman, M.M.; Jang, H.; Ryu, T.; Yoon, S.; Jin, L.; Jin, Y.; Kim, W. Remarkable Conductivity of a Self-Healing Single-Ion Conducting Polymer Electrolyte, Poly(Ethylene- Co -Acrylic Lithium (Fluoro Sulfonyl)Imide), for All-Solid-State Li-Ion Batteries. *ACS Appl. Mater. Interfaces* **2019**, *11*, 34930–34938. [CrossRef]

221. Rohan, R.; Sun, Y.; Cai, W.; Zhang, Y.; Pareek, K.; Xu, G.; Cheng, H. Functionalized Polystyrene Based Single Ion Conducting Gel Polymer Electrolyte for Lithium Batteries. *Solid State Ionics* **2014**, *268*, 294–299. [CrossRef]

222. Feng, S.; Shi, D.; Liu, F.; Zheng, L.; Nie, J.; Feng, W.; Huang, X.; Armand, M.; Zhou, Z. Single Lithium-Ion Conducting Polymer Electrolytes Based on Poly[(4-Styrenesulfonyl)(Trifluoromethanesulfonyl)Imide] Anions. *Electrochim. Acta* **2013**, *93*, 254–263. [CrossRef]

223. Ma, Q.; Zhang, H.; Zhou, C.; Zheng, L.; Cheng, P.; Nie, J.; Feng, W.; Hu, Y.S.; Li, H.; Huang, X.; et al. Single Lithium-Ion Conducting Polymer Electrolytes Based on a Super-Delocalized Polyanion. *Angew. Chem. Int. Ed. Engl.* **2016**, *55*, 2521–2525. [CrossRef]

224. Voropaeva, D.; Novikova, S.; Trofimenko, N.; Yaroslavtsev, A. Polystyrene-Based Single-Ion Conducting Polymer Electrolyte for Lithium Metal Batteries. *Processes* **2022**, *10*, 2509. [CrossRef]

225. Xu, R.; Xiao, Y.; Zhang, R.; Cheng, X.; Zhao, C.; Zhang, X.; Yan, C.; Zhang, Q.; Huang, J. Dual-Phase Single-Ion Pathway Interfaces for Robust Lithium Metal in Working Batteries. *Adv. Mater.* **2019**, *31*, 1808392. [CrossRef] [PubMed]

226. Ruan, Y.; Guo, F.; Liu, J.; Song, S.; Jiang, N.; Cheng, B. Optimization of $Na_3Zr_2Si_2PO_{12}$ Ceramic Electrolyte and Interface for High Performance Solid-State Sodium Battery. *Ceram. Int.* **2019**, *45*, 1770–1776. [CrossRef]